HAL open science

A three-source SVAT modeling of evaporation: Application to the seasonal dynamics of a grassed vineyard

Carlo Montes, Jean-Paul Lhomme, Jérôme Demarty, Laurent Prevot, Frédéric Jacob

To cite this version:

Carlo Montes, Jean-Paul Lhomme, Jérôme Demarty, Laurent Prevot, Frédéric Jacob. A three-source SVAT modeling of evaporation: Application to the seasonal dynamics of a grassed vineyard. Agricultural and Forest Meteorology, 2014, 191, pp.64–80. 10.1016/j.agrformet.2014.02.004 . hal-01863507

HAL Id: hal-01863507

https://hal.science/hal-01863507v1

Submitted on 5 Nov 2021

HAL is a multi-disciplinary open access archive for the deposit and dissemination of scientific research documents, whether they are published or not. The documents may come from teaching and research institutions in France or abroad, or from public or private research centers.

L'archive ouverte pluridisciplinaire **HAL**, est destinée au dépôt et à la diffusion de documents scientifiques de niveau recherche, publiés ou non, émanant des établissements d'enseignement et de recherche français ou étrangers, des laboratoires publics ou privés.

A three-source SVAT modeling of evaporation: application to the seasonal dynamics of a grassed vineyard

Carlo Montes[a*], Jean-Paul Lhomme[a], Jérôme Demarty[b], Laurent Prévot[c] and Frédéric Jacob[a]

[a] Institut de Recherche pour le Développement, UMR LISAH, 34060 Montpellier, France
[b] Institut de Recherche pour le Développement, UMR HSM, 34095 Montpellier, France
[c] Institut National de la Recherche Agronomique, UMR LISAH, 34060 Montpellier, France

[*] *Corresponding author address:*

Carlo Montes, UMR LISAH, 2 place Pierre Viala, 34060 Montpellier, France

E-mail address: ccmontesv@gmail.com

Abstract.

A parsimonious and versatile Soil-Vegetation-Atmosphere Transfer (SVAT) model is proposed for three component vineyards, which includes vine foliage, grassed soil and bare soil. A three-source energy balance approach describes the energy and mass transfer between the soil-plant continuum and the lower atmosphere with an hourly time step. It is coupled with a soil water balance module running with a daily time step. The model makes use of standard meteorological data together with parameters describing foliage development, grass and soil characteristics. The model is calibrated by means of the Multi-objective Calibration Iterative Process (MCIP) algorithm and next validated for evaporation and soil moisture over a dataset collected in a Southern France grassed vineyard. The validation exercise is twofold. It focused first on the daily course of evaporation derived from the surface energy balance module only, forced with weather variables, net radiation and soil moisture. The comparison against Eddy Covariance measurements shows a good agreement (R^2 = 0.96 and RMSE = 14.0 W m^{-2}). Next, a simulation coupling the surface energy balance module with the soil water balance module is validated over Eddy Covariance and soil moisture measurements. Simulations throughout two contrasting growing seasons provide good estimates of daily evaporation (R^2 = 0.90 and RMSE = 0.43 mm d^{-1}) and soil water content (R^2 = 0.98 and RMSE = 6.95 mm). Model inaccuracies arise mainly under conditions of strong surface runoff. Results also suggest that the parameterizations relating the surface-atmosphere module with the soil module (i.e. stomatal resistance) should be carefully examined under water stress conditions. Finally, the model versatility is addressed through a set of static simulations. It appears that the modeling approach allows assessing the seasonal water balance of vineyards differing by their structure (varying grass fraction or distance between rows) and of similar cropping systems.

Key words: latent heat flux; multi-source; sparse vegetation; soil water balance; seasonal course

List of symbols

A_i: available energy for each component *vs* and *bs* (W m^{-2})

A_f: available energy for the main foliage (W m^{-2})

c: radiation extinction coefficient by canopy

c_p: specific heat of air at constant pressure (J kg^{-1} K^{-1})

CR_3: capillary rise into reservoir (3) (mm)

d: displacement height (m)

D_1: drainage from reservoir (1) to (3) (mm)

D_2: drainage from reservoir (2) to (3) (mm)

D_3: deep percolation from reservoir (3) (mm)

D_a: vapor pressure deficit at reference height (Pa)

D_m: vapor pressure deficit at mean canopy source height (Pa)

e_a: vapor pressure at reference height (Pa)

$e^*(T_i)$: saturated vapor pressure at temperature T_i ($i = f$, *vs*, *bs*) (Pa)

F_{bs}: fraction of bare soil (= 1 –F_{vs})

F_{vs}: fraction of vegetated soil

$F_1 = F_{bs}$

$F_2 = F_{vs}$

G_{vs}: soil heat flux of vegetated soil (W m^{-2})

G_{bs}: soil heat flux of bare soil (W m^{-2})

I_{vs}: infiltration term for vegetated soil (mm)

I_{bs}: infiltration term for bare soil (mm)

$K(z_h)$: turbulent diffusivity at canopy height (m^2 s^{-1})

L: Monin-Obukhov length (m)

LAI_f: leaf area index of main foliage (m^2 m^{-2})

$CLAI_{vs}$: clumped leaf area index of vegetated soil (m^2 m^{-2})

n: parameter with value of 1 for amphistomatous and 2 for hypostomatous foliage

r_a: aerodynamic resistance between the mean source height (z_m) and the reference height (z_r, s m^{-1})

$r_{a,i}$: aerodynamic resistance between the evaporative source (i = *vs*, *bs*) and mean source height (z_m, s m^{-1})

$r_{a,f,h}$: bulk boundary-layer resistance of the foliage for sensible heat (s m^{-1})

$r_{s,i}$: surface resistance (stomatal or soil surface) for each source ($i = f$, vs, bs) (s m^{-1})

R_n: net radiation of the whole canopy (W m^{-2})

u_a: wind speed at reference height (m s^{-1})

z_h: height of the main foliage (m)

z_m: mean source height (m)

z_r: reference height (m)

z_0: roughness length for momentum of main foliage (m)

z_0^i: roughness length for momentum of vegetated ($i = vs$) or bare soil ($i = bs$) (m)

z_1: depth of soil reservoir (1) (m)

z_2: depth of soil reservoir (2) (m)

z_R: vines rooting depth (m)

z_G: water table depth (m)

γ: psychrometric constant (Pa K^{-1})

λ: latent heat of vaporization (J kg^{-1})

Δ: slope of the saturated vapor pressure curve at air temperature (Pa K^{-1})

ρ: air density (kg m^{-3})

ϕ_s: solar zenith angle (radians)

1. Introduction

Progress in theoretical and applied research aiming at accurately assessing crop water consumption in both rain-fed and irrigated conditions is an essential issue for agricultural water management. Since evaporation measurements are scarce, operational formulations to estimate water consumption at field scale are necessary (Trambouze et al., 1998; Spano et al., 2009). For viticulture regions in Mediterranean and semi-arid environments, actual evaporation represents a major component of surface water balance, reaching up to 70% of the yearly precipitation (Moussa et al., 2007). Knowledge of actual evaporation is also of interest in viticulture, in order to assess and handle the influence of soil water deficit on grapevine yields and berry composition (Vaudour, 2003; Pellegrino et al., 2005). Nevertheless, the physical representation of the soil-plant-atmosphere system in grapevines is a complex issue, because the sparse structure of vineyards imposes to consider both the foliage and the understory, which requires multi-source modeling.

The most frequently used multi-source evaporation model is the one first developed by Shuttleworth and Wallace (1985) (S-W model) and extended by Choudhury and Monteith (1988) and Shuttleworth and Gurney (1990). This model corresponds to an extension of the big-leaf model of Penman-Monteith (Monteith, 1965) into two interacting evaporative layers: the main foliage and the underlying substrate. Subsequently, the S-W model was upgraded by Brenner and Incoll (1997) ("clumped" model) to account for three sources of evaporation after dividing the understory into a bare soil fraction and a soil fraction below the main foliage, and also by Verhoef and Allen (2000) to account for four sources of evaporation. The two- and three-source formalisms were revisited by Lhomme et al. (2012) to propose more concise and accurate formulations and to account for foliage morphological characteristics (amphistomatous versus hypostomatous leaves). All these models are based on the diffusion theory (*K*-theory) for energy and mass transfer within the lower atmosphere. More complex models based on higher order Lagrangian and Eulerian dispersion processes can be found in the literature: they allow a better representation of vegetation-atmosphere turbulent transfers (Raupach, 1989; Yi, 2008), but their complexity and data requirement make them difficult to use in a practical modeling framework. It has been shown, further, that the diffusion theory is appropriate to represent the microclimate at canopy scale in comparison with Lagrangian representations (van den Hurk and McNaughton, 1995; Wu et al., 2001).

One of the first models to estimate vineyard evaporation is the one proposed by Riou et al. (1989, 1994). It is not a multi-source model: vineyard evaporation under unstressed

conditions is expressed as a simple function of potential evaporation and solar radiation intercepted by the canopy. This model was extended later by Trambouze and Voltz (2001), who derived a bilinear relationship relating the ratio between vineyard actual and maximum transpiration to the average soil water storage. Subsequently, several authors have applied the multi-source resistance-based formulations to assess vineyard evaporation. First, we have to mention the work by Rana and Katerji (2008), where a simple single-source model (Penman-Monteith) was applied to vineyards trained on overhead system. In an earlier work by Sene (1994), the more complex S-W model was applied with the purpose of interpreting energy balance measurements over a sparse vineyard in southern Spain. More recently, an appropriate representation of total latent heat flux from a drip-irrigated vineyard in central Chile was obtained by Ortega-Farias et al. (2007) by applying the same S-W model. In addition, Poblete-Echeverria and Ortega-Farias (2009) adapted the so-called "clumped" model to drip irrigation over the same region of Chile by dividing the substrate (bare soil) into a dry and a wet (irrigated) portion. Zhang et al. (2008) compared these two models (S-W and clumped) against Bowen ratio estimates in a semi-arid vineyard of China: they concluded that the clumped model was more suitable to estimate total vineyard evaporation than the S-W model. On the same basis, Zhang et al. (2009) elaborated a multi-source S-W type model to simulate the evaporation from a vineyard under partial root-zone irrigation, taking into consideration different patches of soil.

All these vineyard evaporation models, however, do not take into account the common practice of maintaining a permanent or semi-permanent grass cover. This consists in a seeded or natural grass cover in between vine rows, maintaining bare soil on the rows. This practice is increasingly used because it has several positive impacts, such as the reduction in rainfall erosive potential and surface runoff, the reduction in nutrient lixiviation, the decrease in vine vigor and grape production (which improves grapes quality) and the improvements in soil structure and trafficability after rainfall events (Pradel and Pieri, 2000; Morlat and Jacquet, 2003; Celette et al., 2005; Celette et al., 2008; Gaudin et al., 2010). As compared with the traditional bare soil grapevine cultivation, the grass cover affects energy and water balance since surface albedo, net radiation partitioning, water consumption and infiltration are modified (Rodriguez-Iturbe, 2000; Zhang and Schilling, 2006; Centinari et al., 2012). For instance, in a recent work by Holland et al. (2013) on grassed vineyard, significant differences were found between grassed and bare soil energy partitioning. Therefore, this grass cover component should be considered into a modelling formulation.

In addition, most of the vineyard evaporation models mentioned above only consider

above-ground processes (i.e. vegetation and soil surface), which interact with soil water through the parameterization of a stomatal or substrate resistance to evaporation, in the best case. Thus, they do not allow the temporal dynamics of vineyard evaporation to be adequately simulated throughout the season. However, models have been developed to simulate soil water balance of vineyards. Sene (1996) was the first to combine a simple soil moisture model with a two-component (S-W) representation of vineyard evaporation in order to estimate the long-term water balance of a sparse vine crop growing under semi-arid conditions. Lebon et al. (2003) also performed simulations of the seasonal dynamics of soil water balance in vineyards by using a single reservoir soil model along with the Riou et al. (1989, 1994) approach for grapevine transpiration coupled with a stress function involving soil water availability (Trambouze and Voltz, 2001). Celette et al. (2010) extended the model of Lebon et al. (2003) to simulate the water balance of an intercropped vineyard considering an additional and separate soil compartment under the cover crop. Galleguillos et al. (2011) also used the model of Riou et al. (1989, 1994), but coupled with the HYDRUS-1D simulation model of soil water transfers. Although realistic results have been obtained with this type of soil water balance model, the evaporation process remains poorly represented and a more realistic approach based upon micrometeorological resistance-type models coupled with soil water models appears to be necessary.

With regards to the elements discussed above, the main objective of the present work is to develop a Soil-Vegetation-Atmosphere Transfer (SVAT) model which simulates the vineyard evaporation dynamics at seasonal scale and accounts for the grass cover as a viticultural practice. It combines a comprehensive micrometeorological three-source model of evaporation with a three reservoir soil water balance model. The formulation is versatile enough to allow the assessment of evaporation rate from different mixed cropping systems, in so far as species-specific biophysical parameters and physical soil properties descriptors are adjusted to the prevailing conditions. The formulation is also kept as parsimonious as possible to foresee its application at the regional extent while accounting for the inter-field variability. The plan is as follows. In Section 2, the SVAT model is fully described, separating the evaporation model from the soil water balance model. Section 3 details the study area, the experimental data, the model implementation and the strategy for calibration. Section 4 shows a comparison of model simulations against ground truth data to validate the model and some simulations are presented to show the versatility of the model through its aptitude to represent different viticultural practices (proportion of grassed soil and distance between rows). Finally, model results and limitations are discussed in Section 5.

2. Model development

2.1 Representing the vine-grass-soil system

The soil-plant-atmosphere continuum is represented as a three-source system that includes the vine canopy (main foliage) and a composite substrate made of a grass cover and bare soil. This rain fed Cabernet Sauvignon vineyard is conducted in rows. Vine leaf area index (LAI_f) varies throughout the growing season from 0 to a maximum value and next falls back to 0 during senescence. The grass cover is present only on one inter-row out of two. It is characterized by the concept of clumped *LAI* ($CLAI_{vs}$), defined as grass leaf area index per unit area of grass cover: $CLAI_{vs} = LAI_{vs}/F_{vs}$, F_{vs} being the proportion of vegetated soil. Grass exhibits a seasonal dynamics: its growth is initiated by autumn precipitations and it dries off in early summer as a result of large water stress. The bare soil fraction (F_{bs}) covers the rest of the inter-row and the soil below the vines. The vine-grass-soil system corresponds to a three-source system between autumn and early summer and to a two-source system in summer, when the substrate is made of bare soil and dry grass only ($F_{bs} = 1$).

The three components should be considered separately because they have different physical and geometrical features which affect energy and mass transfers. Nevertheless, the vine patches are not large enough to adopt a patch representation of the whole system and consequently a layer representation is preferred (Boulet et al., 1999; Lhomme and Chehbouni, 1999; Anderson et al., 2005). Given the composite nature of the substrate, the modeling combines a layer approach for the vine-substrate system with a patch approach for the substrate (grass cover + bare soil), as represented in Fig. 1 and explained in Lhomme et al. (2012, section 3.1). Indeed, while substrate and vine are interrelated in the vertical transfer of heat and water vapor with a sole aerodynamic resistance above the whole canopy, grass cover and substrate are assumed to act separately vis-a-vis the canopy source height.

Soil moisture dynamics is represented by a bucket type model made of three reservoirs in relation with the three components of the evaporation model: a deep reservoir corresponding to the vine rooting system (~2 m) and two shallow reservoirs corresponding to the two substrate components. The main input of the system corresponds to the infiltration of water from precipitation. Drainage processes control the water transfers between reservoirs. Evaporation is the main output and deep percolation acts as a secondary output. Capillary rise from the saturated zone below the deep reservoir is also considered, but horizontal water

transfers (runoff) are ignored.

The SVAT model consists of coupling the surface energy balance for plant-atmosphere system and the soil water balance for the subsurface system. The evaporation model runs with a short time step (one hour or less) and is forced with meteorological data (air temperature and humidity, wind speed, solar radiation) and vegetation data (vine height and leaf area, fraction of grass cover). The soil water balance runs on a daily time step and is forced with daily precipitation. The water content of each subsurface reservoir is an input to the corresponding evaporation components and conversely the evaporation components are inputs for the soil water balance module.

2.2 Evaporation model

We detail hereafter the surface energy balance and soil water balance modules forming the SVAT model and their corresponding parameterizations. For the numerous formulations considered in this section, the values of the corresponding parameters are given in Table 1.

2.2.1 Formulation of evaporation

The total flux of latent heat (λE_t) is the sum of the contributions from three sources: main foliage (λE_f), vegetated soil (λE_{vs}) with relative area F_{vs} and bare soil (λE_{bs}) with relative area $F_{bs} = 1 - F_{vs}$. They are aggregated following a coupled (or layer) approach (Fig. 1):

$$\lambda E_t = \lambda E_f + \lambda E_{vs} + \lambda E_{bs}. \quad (1)$$

The three evaporation components reach the mean canopy source height (z_m), assumed to be located at the apparent sink for momentum (zero plane displacement height d + roughness length z_0), where they mix together forming the total evaporation at reference height (z_r) as it can be measured with Bowen ratio or Eddy Covariance system. The resistances network represents the controlling effects of soil surface, stomatal behavior and surrounding air, which are considered to be "in series" for each individual source. Vegetated (vs) and bare soil (bs) air resistances extend from the surface level ($z_{0,i}$, i = vs or bs) to the mean canopy source height (z_m). Evaporation components are calculated from Penman-Monteith type equations

involving the corresponding available energy (A_f, A_{vs} or A_{bs}) and the vapor pressure deficit D_m at mean canopy source height z_m. However, following Lhomme et al. (2012), the stomatal characteristics of the main foliage (amphistomatous or hypostomatous) are taken into account in the evaporation formulation

$$\lambda E_f = \frac{\Delta A_f + \rho c_p D_m / r_{a,f,h}}{\Delta + \gamma\left(n + r_{s,f} / r_{a,f,h}\right)}, \tag{2}$$

where the parameter n takes the value $n = 1$ for amphistomatous and $n = 2$ for hypostomatous leaves. Since grapevine foliage is hypostomatous, we took $n = 2$. Δ is the slope of the saturated vapor pressure curve at air temperature, ρ the air density, c_p the specific heat of air at constant pressure, γ the psychrometric constant, $r_{a,f,h}$ the foliage bulk boundary-layer resistance for sensible heat and $r_{s,f}$ the bulk surface resistance of the foliage. For the two substrate components (vegetated soil and bare soil) we have

$$\lambda E_i = \frac{\Delta A_i + \rho c_p D_m / r_{a,i}}{\Delta + \gamma\left(1 + r_{s,i} / r_{a,i}\right)}, \qquad \text{with } i = vs \text{ or } bs \tag{3}$$

$r_{a,i}$ is the aerodynamic resistance between the evaporative source ($i = vs$, bs) and z_m, and $r_{s,i}$ is the surface resistance (stomatal or soil surface) for each source ($i = vs$, bs).

The total evaporation per unit area from the whole canopy is obtained using the formulation developed by Lhomme et al. (2012, Eq. (33)) for a three-source evaporative surface:

$$\lambda E_t = \left(\frac{\Delta + \gamma}{\gamma}\right)\left(P_f + P_{vs} + P_{bs}\right)\lambda E_p + \frac{\Delta}{\gamma}\left(P_f r_{a,f,h} A_f + P_{vs} r_{a,vs} A_{vs} + P_{bs} r_{a,bs} A_{bs}\right) / r_a, \tag{4}$$

where λE_p represents the potential evaporation expressed as

$$\lambda E_p = \frac{\Delta A + \rho c_p D_a / r_a}{\Delta + \gamma}, \tag{5}$$

where A is the total available energy and r_a is the aerodynamic resistance between the source height z_m and the reference height z_r. The P_i coefficients of Eq. (4) are combinations of surface and aerodynamic resistances, detailed in Appendix A. Each evaporation component is obtained from Eqs. (2) and (3) by expressing the in-canopy vapor pressure deficit D_m as a function of the saturation deficit at reference height D_a (Shuttleworth and Wallace, 1985):

$$D_m = D_a + \left[\Delta A - \lambda E_t(\gamma + \Delta)\right] r_a / (\rho c_p). \tag{6}$$

2.2.2 Partition of available energy

Total available energy (A) for turbulent fluxes is defined as the difference between the total net radiation (R_n) and the soil heat flux (G) counted positively when gained by the surface: $A = R_n - G$. Beer's law is used to obtain the partitioning of net radiation including the effects of solar zenith angle (ϕ_s) on net radiation extinction (Anderson et al., 1997; Kustas et al., 1998). Considering the canopy as a semi-transparent layer to incident radiation, the net radiation reaching the substrate level $R_n(0)$ is obtained by

$$R_n(0) = R_n \exp\left(-cLAI_f / \sqrt{2\cos(\phi_s)}\right), \tag{7}$$

where c is the extinction coefficient of radiation of the main foliage, which depends upon leaves angular distribution (Choudhury, 1989), and LAI_f its leaf area index. For the main vegetation canopy, the available energy (A_f) is computed as the difference between the total net radiation above the canopy and that reaching the substrate level:

$$A_f = R_n - R_n(0) = R_n\left[1 - \exp\left(-cLAI_f / \sqrt{2\cos(\phi_s)}\right)\right]. \tag{8}$$

Soil heat flux for vegetated and bare soil (G_{vs} and G_{bs}, respectively) is obtained as a fraction of the net radiation reaching the substrate level (Norman et al., 1995; Boulet et al., 2000). Per unit area of substrate we have $G_{vs} = \beta_{vs} R_n(0)$ and $G_{bs} = \beta_{bs} R_n(0)$, β_{vs} and β_{bs} representing the proportions of residual net radiation conducted into the soil. Available energy for vegetated (A_{vs}) and bare soil (A_{bs}) is respectively obtained as

$$A_{vs} = F_{vs}\left[R_n(0) - G_{vs}\right] = F_{vs}(1-\beta_{vs})\exp\left(-cLAI_f \Big/ \sqrt{2\cos(\phi_s)}\right)R_n, \tag{9}$$

$$A_{bs} = F_{bs}\left[R_n(0) - G_{bs}\right] = F_{bs}(1-\beta_{bs})\exp\left(-cLAI_f \Big/ \sqrt{2\cos(\phi_s)}\right)R_n, \tag{10}$$

and consequently

$$A = R_n - G = R_n\left[1 - \exp\left(-cLAI_f \Big/ \sqrt{2\cos(\phi_s)}\right)\left(F_{vs}\beta_{vs} + F_{bs}\beta_{bs}\right)\right]. \tag{11}$$

2.2.3 Net radiation estimation

The evaporation formulations detailed in Section 2.2.1 consider that the net radiation of the whole surface constitutes an input to the model. It is expressed as

$$R_n = (1-a)R_g + \varepsilon\left(R_{atm} - \sigma T_R^4\right), \tag{12}$$

where a is the effective surface albedo, R_g the incoming shortwave or solar radiation, R_{atm} the downward longwave or atmospheric radiation, ε the surface longwave emissivity, σ the Stefan-Boltzmann constant and T_R the composite radiometric temperature of the surface (main foliage and substrate).

Net radiation, however, is not commonly and routinely measured. Given that the purpose of this work is to develop an operational and dynamic version of the model running with meteorological inputs, R_n should be determined beforehand. If R_g is generally measured and R_{atm} measured or easily calculable from air temperature and humidity, T_R is an unknown variable which cannot be considered as an input to the model. It can be expressed as a function of the component temperatures in the following way based on the Stefan-Boltzmann law (Norman et al., 1995):

$$T_R = \left[f_0 T_f^4 + (1-f_0)T_s^4\right]^{1/4}, \tag{13}$$

where T_f is the temperature of the main foliage and T_s is the composite substrate temperature expressed as a weighted mean of the component temperatures

$$T_s = F_{vs}T_{vs} + F_{bs}T_{bs}. \tag{14}$$

In Eq. (13) f_0 represents the fractional vegetation cover obtained by

$$f_0 = 1 - \exp\left(-cLAI_f\right), \tag{15}$$

with c the same coefficient as in Eq. (7) and LAI_f the leaf area index of the main foliage. Given that surface temperature T_R is required to solve Eq. (12), an iterative procedure is implemented to obtain the corresponding surface temperatures (T_f, T_{vs}, T_{bs}). An initial loop sets $T_i = T_a$ ($i = f$, vs, bs) to solve Eqs. (12) to (15) and to calculate the distribution of available energy from Eqs. (7) to (11). Eqs. (4) to (6) are then used to calculate λE_t and D_m, which allows calculating a new set of component surface temperatures T_i, which are reintroduced into Eq. (13) until the convergence is achieved. The details of surface temperatures calculation are presented in Appendix B.

The effective albedo for shortwave radiation (a in Eq. (12)) is obtained using the following expression (Taconet et al., 1986; Lhomme and Monteny, 2000):

$$a = f_0 a_f + \frac{a_s\left(1 - f_0\right)^2}{\left(1 - f_0 a_f a_s\right)}, \tag{16}$$

where a_f and a_s are the albedos of the main foliage and of the substrate, respectively. Substrate albedo a_s is calculated as a simple weighted component albedo: $a_s = F_{bs}a_{bs} + F_{vs}a_{vs}$, with a_{vs} and a_{bs} the albedo of the vegetated and bare soil, respectively.

2.2.4 Parameterizations of surface and aerodynamic resistances

Surface resistances

The main foliage surface resistance to vapor transfer is parameterized using the widely used Jarvis-type analytical formulation (Jarvis, 1976). This formulation links the stomatal conductance (inverse of resistance) to environmental factors controlling the relative stomatal closure: photosynthetically active radiation (PAR_f), vapor pressure deficit (D_a) and soil water

content (θ_f). It is expressed as

$$g_{s,f} = 1/r_{s,f} = \left(g_{x,f} LAI_f\right) f_1\left(PAR_f\right) f_2\left(D_a\right) f_3\left(\theta_f\right), \tag{17}$$

where $g_{x,f}$ is the maximum leaf stomatal conductance, observed when environmental factors are not limiting. Each function represents a stress function with values between 0 and 1. They are defined as

$$f_1\left(PAR_f\right) = 1 - \exp\left(-PAR_f / K_1^f\right), \tag{18}$$

$$f_2\left(D_a\right) = 1 - K_2^f D_a, \tag{19}$$

where PAR_f is the photosynthetically active radiation reaching the main foliage (calculated as a fraction of solar radiation); K_1^f and K_2^f are two empirical parameters. The stress function for soil water content is parameterized considering a negative exponential relationship between stomatal conductance and soil water deficit (Stewart, 1988). This relationship is defined as

$$f_3\left(\theta_f\right) = 1 - \exp\left[-K_3^f\left(\theta_f - \theta_{f,wp}\right)\right], \tag{20}$$

with θ_f the volumetric soil moisture averaged over the depth of the rooting system, $\theta_{f,wp}$ its moisture at wilting point and K_3^f a fitting parameter.

Grass cover conductance is calculated using the same formulation as above (subscript *f* is replaced by subscript *vs*), but with specific parameters and coefficients. However, since grass occupies only a portion of the representative area (F_{vs}), the stomatal conductance should be multiplied by this relative area (Lhomme et al., 2012). Local observations indicate that the inter-row grass cover extends its vegetative cycle until early summer and then completely dries out, which means that stomatal conductance becomes equal to zero and only soil evaporation should be considered, then F_{vs} is set to zero.

Direct evaporation from topsoil layers is regulated by complex processes that can be summarized in a soil surface resistance $r_{s,bs}$. A wide list of formulations for this physical

control on evaporation can be found in the literature, most of them relating $r_{s,bs}$ to local observations of soil water content (e.g. Mahfouf and Noilhan 1991). This resistance was parameterized using the formulation proposed by Sellers et al. (1992), divided by bare soil relative area:

$$r_{s,bs} = \exp\left(A_1 - B_1\, \theta_{bs} / \theta_{s,bs}\right) / F_{bs}\,, \tag{21}$$

with θ_{bs} and $\theta_{s,bs}$ the actual and saturated water content of the upper soil layer; A_1 and B_1 are fitting parameters.

Aerodynamic resistances

The aerodynamic resistance between canopy source height (z_m) and reference height (z_r), assumed to be the same for heat and water transfer, is calculated using the formulation proposed by Brutsaert (1982), which takes into account the stability correction functions for momentum and heat under non-neutral conditions. The boundary layer resistance of the main foliage is estimated using the formulation proposed by Choudhury and Monteith (1988). The aerodynamic resistances between the substrate and the mean canopy source ($r_{a,vs}$ and $r_{a,bs}$) are defined by the integral of the inverse of the eddy diffusivity (Choudhury and Monteith, 1988; Shuttleworth and Gurney, 1990). All these aerodynamic resistances are detailed in Appendix C. For substrate components, the aerodynamic resistances should be weighted by their relative area, as highlighted by Lhomme et al. (2012). If $r^1_{a,i}$ (i = vs, bs) is the aerodynamic resistance per unit area of component substrate with relative area F_i, the aerodynamic resistance per unit area of land surface should be written as $r_{a,i} = r^1_{a,i} / F_i$.

2.3 Water balance model

2.3.1 Soil water equations

To simulate the water budget seasonal dynamics, the evaporation model described in section 2.2, which is run with an hourly time step, is coupled with a soil water balance module run with a daily time step. The daily time step was selected for feasibility reasons, since daily

values of rainfall are usually more available than hourly values. The soil layer beneath the vegetation is divided into three finite reservoirs (Fig. 1): a reservoir (1), located just below the bare soil component with relative area $F_1 = F_{bs}$ and depth z_1; reservoir (2), located just below the vegetated soil with relative area $F_2 = F_{vs}$ and depth z_2; and reservoir (3), located below reservoirs (1) and (2), which extends to a depth z_R taken as equal to the vines rooting depth. Available water content of each soil compartment is considered as uniformly distributed over the corresponding soil profile. Bare soil and vegetated soil evaporation occur respectively from reservoir 1 and 2. Main foliage is supposed to extract water both from reservoirs 2 and 3, because the rooting system of vines is expected to extend within that of grass. A saturated zone with depth z_G is also considered, which potentially can rise to reach the bottom of reservoir (3).

Horizontal water transfers, as well as surface runoff, are considered out of the scope of this one-dimensional modeling approach and are ignored. In any case, the runoff component can be added (or subtracted) to the infiltration term of the water balance. Thus, the main water input to the system corresponds to the infiltration of water from precipitation to reservoirs (1) and (2). Root water uptake by the vineyard and grass, and bare soil evaporation correspond to the main water outputs. Transfers from reservoirs (1) and (2) to (3), and from (3) to the saturated zone are carried out through percolation process. Capillary rise from the saturated zone to reservoir (3) can also act as a secondary input of water. Capillary rise from reservoir (3) to surface reservoirs (1) and (2) is assumed to be negligible.

Soil water capacity TSW_i (total soil water) for each reservoir is defined as the difference between the amount of water stored at field capacity and a minimum amount, specified below. It is calculated as a function of its depth and relative area F_i

$$TSW_i = 1000 F_i z_i \left(\theta_{fc,i} - \theta_{n,i}\right)\left(1 - p_i\right), \qquad i = 1 \text{ or } 2 \tag{22}$$

$$TSW_3 = 1000\left[F_2\left(z_R - z_2\right) + F_1\left(z_R - z_1\right)\right]\left(\theta_{fc,3} - \theta_{n,3}\right)\left(1 - p_3\right), \tag{23}$$

TSW_i is expressed in mm and the reservoir depth z_i in m, θ_i is the volumetric humidity in $m^3\ m^{-3}$ (subscript *fc* indicates field capacity and *n* a minimum value), p_i is the fractional stone content, and the value 1000 is a conversion factor. Similarly, available soil water (ASW_i) of each reservoir is defined as the difference between its actual water content (θ_i) and its content at a minimum value ($\theta_{n,i}$). It is expressed by the same equations as (22) and (23), where $\theta_{fc,i}$ is

replaced by θ_i. For reservoir (2) the minimum humidity ($\theta_{n,2}$) is taken to be equal to that at wilting point ($\theta_{vs,wp}$). For reservoirs (1) and (3), the minimum humidity $\theta_{n,i}$ is set to minimum values below wilting point, as observed by Trambouze and Voltz (2001) on the same plot (Table 2).

The root system of the main vegetation is supposed to extract water from compartments (1) and (2). The grass cover extracts water only from reservoir (2) and bare soil evaporation comes from reservoir (1) which is only a few centimeters deep. The amount of water (ASW_i) stored into each of the three compartments is calculated following a dynamic process with a daily budget (subscript j):

$$ASW_{1,j} = ASW_{1,(j-1)} + I_{1,j} - E_{1,bs,j} - D_{1,j}, \tag{24}$$

$$ASW_{2,j} = ASW_{2,(j-1)} + I_{2,j} - E_{2,vs,j} - E_{2,f,j} - D_{2,j}, \tag{25}$$

$$ASW_{3,j} = ASW_{3,(j-1)} + I_{3,j} + CR_{3,j} - E_{3,f,j} - D_{3,j}. \tag{26}$$

The infiltration terms are denoted by I, the percolation terms by D and the evaporation terms by E. All the terms are expressed in mm d^{-1}. The water inputs for vegetated and bare soil reservoirs are daily rainfall (P_j) weighted by their relative area (F_i), so $I_{i,j} = F_i P_j$ (i = 1 and 2). The infiltration into the third reservoir ($I_{3,j}$) is expressed as the sum of the drainage components of the upper reservoirs as $I_{3,j} = D_{1,j} + D_{2,j}$. For each reservoir, percolation is calculated as the amount of water in excess with respect to the total available water: it is the positive difference between the sum of inputs and the water holding capacity of the reservoir defined as the difference between TSW_i and ASW_i. For the surface compartments (i= 1 and 2) we have

$$D_{i,j} = I_{i,j} - \left(TSW_i - ASW_{i,j}\right) \quad \text{if} \quad I_{i,j} > \left(TSW_i - ASW_{i,j}\right), \tag{27}$$

$$D_{i,j} = 0 \quad \text{if} \quad I_{i,j} \le \left(TSW_i - ASW_{i,j}\right), \tag{28}$$

and for compartment (3)

$$D_{3,j} = \left(D_{1,j} + D_{2,j}\right) - \left(TSW_3 - ASW_{3,j}\right) \quad \text{if} \quad \left(D_{1,j} + D_{2,j}\right) > \left(TSW_3 - ASW_{3,j}\right), \tag{29}$$

$$D_{3,j} = 0 \quad \text{if} \quad \left(D_{1,j} + D_{2,j}\right) \leq \left(TSW_3 - ASW_{3,j}\right). \tag{30}$$

Given that the evaporation module is run with a time step shorter than one day (e.g. 1 hour), the evaporation terms are calculated as the 24 hours summation. The partitioning of main foliage evaporation between the two compartments (2) and (3) is obtained through a simple weighting by the relative soil water content of these two compartments. Putting $ASW_f = ASW_2 + ASW_3$, we have respectively

$$E_{2,f,j} = \frac{ASW_2}{ASW_f} \sum_{h=1}^{24} E_{f,j,h} \quad \text{and} \quad E_{3,f,j} = \frac{ASW_3}{ASW_f} \sum_{h=1}^{24} E_{f,j,h}, \tag{31}$$

where $E_{f,j,h}$ is the evaporation from the main foliage in mm h^{-1}. In Eq. (31), evaporation components E_f, E_{vs} and E_{bs} are obtained by Eqs. (2) and (3).

Since the main foliage extracts water from compartments (2) and (3), the soil water content (θ_f) involved in its stress function (Eq. (20)) is calculated as the mean of the water contents of both compartments weighted by their relative volume:

$$\theta_f = \frac{V_2\theta_2 + V_3\theta_3}{V_2 + V_3}, \tag{32}$$

where the volumes of compartments (2) and (3) are calculated respectively as $V_2 = F_{vs} z_2$ and $V_3 = F_{bs}\left(z_R - z_1\right) + F_{vs}\left(z_R - z_2\right)$. The stress function for the vegetated soil simply involves $\theta_{vs} = \theta_2$.

2.3.2 Capillary rise

The upward flow of groundwater to the root zone by capillary rise is driven by the soil hydraulic properties, the vertical gradient of water potential and the depth of the saturated zone (Maxwell and Miller, 2005; Vervoort and van der Zee, 2008), with high nonlinearities involved (Bogaart et al., 2008). When the water table is shallow, the increase in soil moisture

of the root zone induced by the upward flow from the saturated zone can directly influence the magnitude and seasonal course of evaporation (Guix-Hébrard et al., 2007; Soylu et al., 2011). In the present work, the upward transfer of water by capillary rise (CR_3) from the saturated zone to reservoir (3) is estimated using a bulk form of Darcy's law, which considers the flow of water proportional to the difference of water potential and inversely proportional to the distance between reservoirs

$$CR_3 = K_{G,3}\left(\frac{\Psi_{s,G} - \Psi_3}{\Delta z_{G,3}}\right), \tag{33}$$

where $\Psi_{s,G}$ is the water potential of the saturated zone (Clapp and Hornberger, 1978), $\Delta z_{G,3}$ is the distance between the top of the saturated zone (z_G) and the bottom of reservoir (3) (z_R), and $K_{G,3}$ the soil hydraulic conductivity of the transition zone between z_G and z_R (Fig. 1). The water potential of unsaturated soil is the sum of pressure potential and gravitational potential taking the reference height at water table level $\Psi_3 = \Psi_{p,3} + (z_G - z_R)$. Pressure potential $\Psi_{p,3}$ and hydraulic conductivity are determined as a function of soil water content θ_3 following Campbell (1974) and Clapp and Hornberger (1978)

$$\Psi_{p,3}(\theta) = \frac{\Psi_{s,3}}{\left(\theta_3 / \theta_{s,3}\right)^{b_3}}, \tag{34}$$

where the parameters $\Psi_{s,3}$, $\theta_{s,3}$ (water potential and soil water content for saturated conditions) and b_3 (a pore size distribution index) are given by Clapp and Hornberger (1978) according to soil properties. The unsaturated hydraulic conductivity of the transition zone ($K_{G,3}$) between the top of the water table and the bottom of reservoir (3) is a power function of soil moisture content of this transition zone between z_R and z_G (Campbell, 1974). Since this moisture content is a priori unknown, the same value as reservoir (3) is considered

$$K_{G,3} = K_{s,3}\left(\frac{\theta_3}{\theta_{s,3}}\right)^{2b_3+3}, \tag{35}$$

$K_{s,3}$ is the hydraulic conductivity under saturated conditions. Finally, Darcy's law can be rewritten in a bulk form as

$$CR_3 = K_{G,3}\left[\left(\frac{1}{z_G - z_R}\right)\left(\Psi_{s,G} - \frac{\Psi_{s,3}}{\left(\theta_3/\theta_{s,3}\right)^{b_3}}\right) - 1\right], \tag{36}$$

where $\Psi_{s,G}$ is the water potential of the saturated zone (Clapp and Hornberger, 1978), the values of θ_3 being given by the soil water balance model at each time step.

3. Experiment and model implementation

3.1 Study area

The experiment took place in the vineyard watershed of the Peyne river, a tributary of the Hérault river, located in the Languedoc-Roussillon region of southern France. The climate is Mediterranean, with an average annual precipitation of 650 mm, mainly concentrated during autumn and spring, and a dry summer season. Average annual reference evaporation is 1105 mm. Soil was a Cambisoil (clayic) with a 2.3 to 2.5 m depth.

Measurements were carried out on flat vineyard (*Vitis vinifera* L.) of 13 hectares located at 43.4739ºN 3.3697ºE, with an elevation of 42 m.a.s.l. The inter-row distance was 2.5 m and intra-row plant distance was 1 m. Vine canopy height and width was maintained at 1.5 m and 1 m, respectively, by regular thinning. The maximum value of vine LAI_f was 3. The natural grass cover is characterized by a fractional area F_{vs} = 0.3 and $CLAI_{vs}$ = 2 (Paré, 2011).

3.2 Data collection

Hourly values of solar radiation, air temperature, relative humidity, wind speed and rainfall were continuously obtained from a CIMEL Enerco 400, following meteorological standards, apart from wind speed (measured at 2 m height rather than 10 m for agrometeorological purposes). This weather station was located 4.4 km east-northeast of the vineyard.

Components of the energy balance were measured by using a portable micro meteorological station equipped with a Young 81000 3D sonic anemometer (R.M. Young,

USA), a fast hygrometer KH20 (Campbell Inc., USA) and a net radiometer NRlite (Kipp-Zonen, NLD), installed at 2.8 m above ground. An air temperature and relative humidity probe HMP45C (Campbell Inc., USA) allowed correcting for the calibration drift of the KH20. Three soil heat flux plates HFP01 (Huskeflux, NLD) were installed at 0.05 m below the soil surface. This flux station was installed 10 times (3 in 2007, 7 in 2008) in the middle of the vineyard, for 2-4 days periods. Raw data Eddy Covariance (EC) (wind speed components, air temperature and humidity) were acquired at 20 Hz. Other data were acquired at 1Hz and stored as 15 minutes averages.

Soil moisture data were obtained from a Vectra 503-DR CPN Neutron Probe (NP) device. Soil moisture profile was sampled every 0.2 m between 0.2 and 2.5 m of soil depth. This was performed biweekly and after significant rainfall events. The top 0.15 m layer was monitored using a Soil Moisture Equipment TRASE 6050 Time Domain Reflectometry sensor. Soil physical properties measured along the soil profile were averaged and weighted by the corresponding horizon thickness in order to obtain a single value of actual water content (θ), wilting point (θ_{wp}), field capacity (θ_{fc}), stone content (p) and constants for each reservoir. Manual piezometric measurements conducted concurrently to the soil moisture profiles demonstrated the absence of watertable in the first four meters.

Vines were monitored for height and leaf area was estimated during the period of maximum growth using hemispherical photographs processed using the CAN_EYE software. Further details on this experiment can be found in Galleguillos et al. (2011).

3.3 Model forcing

In context of developing a versatile and parsimonious SVAT model devoted to the characterization of vineyard water consumption, the required forcing data are conventional meteorological observations such as those collected during the experiment (air temperature, relative humidity, global radiation, wind speed and daily-accumulated rainfall, see Section 3.2). Atmospheric radiation is estimated from available meteorological data through the parameterization proposed in Appendix D, but direct measurements can be used when existing.

The leaf area index of the vine foliage (LAI_f) is required as input variable in several parameterizations (i.e. available energy components, air and surface resistances), whereby a time series of LAI_f is required. The seasonal evolution of LAI_f is simulated as a function of thermal time by means of a double logistic relationship (Clevers et al., 2002; Fisher et al.,

2006). In this approach, LAI_f rises up to a plateau and then decreases when senescence begins (Fig. 2k-2l). It is calculated as

$$LAI_f(TT) = \left(LAI_{f,\max} - LAI_{f,\min}\right)\left(\frac{1}{1+\mathrm{e}^{m_1+m_2(TT-TT_1)}} - \frac{1}{1+\mathrm{e}^{m_3+m_4(TT-TT_2)}}\right) + LAI_{f,\min}, \quad (37)$$

with $LAI_{f,\max}$ and $LAI_{f,\min}$ the maximum and minimum values of LAI_f during the growing season, respectively; TT is the thermal time calculated with a daily time step

$$TT = \sum \max\left(\frac{T_{\max} + T_{\min}}{2} - T_b, 0\right), \quad (38)$$

where $T_{\max}$ and $T_{\min}$ are the daily maximum and minimum temperatures (ºC), respectively, and T_b a base temperature below which plant growth is negligible, considered typically as 10 ºC for grapevine (Winkler and Williams, 1939). In Eq. (37) m_1 and m_2 are fitting parameters that control the growth stage, m_3 and m_4 are those for the senescence stage, TT_1 and TT_2 represent empirical values that drive the beginning and ending of the vegetative cycle. The values of the parameters were obtained by applying a basic fitting procedure considering the vegetation data collected over the 2008 season: the value of $LAI_{f,\max}$ and the observed dates of three foliage stages (beginning of growth, maximum growth and beginning of senescence). The thermal summation began from 01-March-2008 (taking $LAI_{f,\min} = 0$) and the values found were: $TT_1 = 800$, $TT_2 = 2500$, $m_1 = 0.01$, $m_2 = 0.07$, $m_3 = 0.01$ and $m_4 = 0.05$.

The grass cover is assumed to be already green and covering at the beginning of the seasonal cycle and to be completely senescent if a dry spell of seven consecutive days without available soil water ($ASW_2 = 0$) occurs (Paré, 2011). When this event occurs, only bare soil evaporation is considered during the following days ($F_{vs} = 0$). Local observations suggest that the grass cycle restarts after the grape harvest.

3.4 Model calibration

As for most SVAT models, the correct implementation of the three-source model described above depends upon the appropriate specification of the controlling parameters. They are often difficult to obtain empirically by local fitting and a wide variation in their

values is found in the literature. Moreover, their transferability to different environmental conditions should be handled with care at the risk of systematic errors.

In the present work, a total of 31 parameters have to be defined first. Given the wide range of values found in the literature and the lack of local observations, a total of 16 parameters related to energy balance and surface resistances (listed in Table 1) were obtained by calibration, whereas a total of 15 soil-related parameters were obtained by local observation (soil profile description) or direct consultation of the literature in the case of capillary rise equations (Table 2). The calibrated parameters were calculated by applying the Multi-objective Calibration Iterative Procedure (MCIP) algorithm developed by Demarty et al. (2004, 2005). This multi-criteria global calibration method is based on the minimization of a cost function describing the model performance in relation to field observations. Thus, starting from an initial uncertainty range for each parameter (Table 1), an iterative procedure is carried out to reduce the feasible parameter space by optimization of model outputs against observations. Bastidas et al. (1999), Gupta et al. (1999) and Demarty et al. (2004, 2005) provide detailed description of this multi-objective calibration approach, and several works in land-surface models calibration have used this stochastic method, namely Coudert et al. (2006), Saux-Picart et al. (2009) and Guillevic et al. (2012).

In an algorithmic way, for each iteration, the MCIP method can be summarized as follows: (1) based on local measurements and literature, the initial feasible parameter space is defined (Table 1); (2) the parameter space is uniformly sampled and a set of Monte Carlo random simulations is performed for each parameter combination (2000 in our case); (3) the corresponding cost functions are calculated for every single simulation, in this case using the root mean square errors (RMSE[†]) between model estimates and observed values; (4) using the Pareto ranking approach, or a simple sorting when only one objective function is calculated, the resulting cost function ensemble is partitioned into acceptable and non-acceptable solutions according to a prescribed cost functions threshold; (5) a sensitivity analysis of model parameters is performed based on the MOGSA algorithm (Bastidas et al., 1999), which consists in carrying out the non-parametric test of Kolmogorov-Smirnov to statistically compare the empirical cumulative distribution of model parameters between the acceptable and non-acceptable solutions; and (6) the parameter space is contracted for those parameters with significant differences between the two samples (i.e. sensitive parameters) found in (5),

[†] $\mathrm{RMSE} = \sqrt{\sum_1^n (e_i - m_i)^2 / n}$, with e_i the estimated value and m_i the observed value at time step i

and then a new set of simulations is performed. Parameters found as no sensitive are left to vary freely in the *a priori* uncertainty range of the precedent iteration. These steps are executed iteratively (10 iterations in our case) in order to narrow the parameter range until an optimized set of parameters is obtained.

In the present work, this methodology was applied to obtain an optimized set of parameters belonging to the plant-atmosphere module (Table 1), soil parameters being set as constant during the calibration procedure (Table 2). In this way, total latent heat flux was simulated and the cost function (RMSE) was minimized for a total of eight selected days where both evaporation and soil water content measurements were available. Initial soil water content of the three reservoirs was set by correcting the first observed value by the cumulative evaporation of the previous days.

4. Results

The simulation period is constrained by the data availability, comprising the growing season from 25-July through 30-September in 2007 and from 10-April through 30-September in 2008. The time series of meteorological data used for model forcing during the simulation period are shown in Fig. 2a-2j. The time series of LAI_f obtained with Eq. (37) and $CLAI_{vs}$, both used for model forcing, are shown in Fig. 2k-2l. Local information from growers indicates that, given vineyard pruning, $LAI_{f,\max}$ can be taken as the same for 2007 and 2008 seasons, so the same curve was used in both simulation periods. A contrasting soil water recharge was observed during these two periods: the 2007 season was characterized by dryer conditions, with 262 mm (versus 321 mm in 2008) of cumulated rainfall from April through September. Furthermore, the fall and winter precipitations preceding the vineyard growing seasons provided a lower load in 2007 than in 2008: 173 mm versus 306 mm from October to March.

In the first part of this section, the values of the parameters obtained with the MCIP algorithm are presented and analyzed. The second part addresses the validation of the diurnal course of hourly evaporation derived from the surface energy balance module only, as forced with measurements of net radiation and soil moisture. In the third part, the whole model, including both the surface energy balance and the soil water balance, is validated on simulations of water balance at a daily time step. Finally, the model versatility is explored by analyzing the impact of capillary rise and vineyard structure on total evaporation and soil

water balance.

4.1 Analyzing calibrated parameters

The values of the parameters of the plant-atmosphere module inferred from the MCIP algorithm are shown in Table 1. There are two types of parameters: a set of biophysical parameters obtainable from measurements and another one corresponding to fitting empirical coefficients. Checking the pertinence and accuracy of the first set of optimized values is necessary. Very few references in the literature report measurements of these parameters for vineyards.

The attenuation coefficient of the vineyard foliage for net radiation c = 0.45 was obtained by the MCIP algorithm. In the literature there is a large range of values for this parameter. Sene (1994) proposed c = 0.68 for a different type of vineyard grown in southern Spain and characterized by free standing bushes with a higher aerial biomass. This value was also used by Zhang et al. (2008) in China. The value c = 0.38 was obtained by Poblete-Echeverria and Ortega-Farias (2009) and c = 0.5 by Ortega-Farias et al. (2007) for vineyards in central Chile. These last values are closer to that found here (c = 0.45), likely due to a higher similarity with the vineyards trained in trellis system for the same variety under Mediterranean-type conditions.

The maximum stomatal conductance calculated by the MCIP algorithm was $g_{x,f}$ = 3.3x10^{-3} m s^{-1}. This value is fairly realistic since it is within the range of values measured by Winkel and Rambal (1990) (1.25x10^{-3} m s^{-1}), Lebon et al. (2003) (2.86x10^{-3} m s^{-1}), Zhang et al. (2008) (6.85x10^{-3} m s^{-1}), Ortega-Farias et al. (2010) (6.94x10^{-3} m s^{-1}) and also close to the daytime average value found by Ortega-Farias et al. (2007) on irrigated vineyard (2.13x10^{-3} m s^{-1}). Also, Jones et al. (2002) found an average $g_{x,f}$ = 4.0x10^{-3} between shaded and sunlit leaves in irrigated vineyard. For the grass cover, its Mediterranean type can explain the lower value retrieved for its maximal stomatal conductance $g_{x,vs}$ than the daytime average value of Allen et al. (1989) ($g_{x,vs}$ = 1.0x10^{-2} m s^{-1}).

The relatively large dispersion observed in the measured values of $g_{x,f}$ and c reveals the difficulty to find adequate values for model parameters and justifies the use of a stochastic approach. Conversely, a smaller variability is observed for vineyard albedo. The optimized value a_f = 0.24 is close to those found by Sene et al. (1994) (a_f = 0.27), Pieri and Gaudillère (2003) (a_f = 0.2) and Ortega-Farias et al. (2010) (a_f = 0.19). On the other hand, optimized substrate albedos (a_{bs} = 0.3 and a_{bs} = 0.25) are very close to those often found in the literature

for dry and grassed soils (e.g. Idso et al., 1975; Grasser and van Babel, 1982; Davies, 2006). The differences are ascribed to different substrate composition.

Finally, when dealing with soil heat flux estimation, the retrieved fraction β_{bs} for bare soil is higher than β_{vs} for vegetated soil, which is in agreement with the thermal properties of both covers.

4.2 Evaporation estimates

In this section, the evaporation model is evaluated alone, without being coupled with the soil water balance module. Measurements of soil water content and net radiation are used as input data for Eq. (20) and Eqs. (7) to (11), respectively, in order to evaluate the three-source scheme itself, independently of its operational utilization on a seasonal basis. The model performance in terms of simulated daily course of total evaporation is compared against a set of EC measurements during the contrasting environmental conditions of 2007 and 2008, which constitutes an assessment of the residual calibration error. A comparison between the SVAT model outputs and the set of hourly EC measurements is shown in Fig. 3, including the agreement evaluation by using the root mean square error (RMSE), the bias estimation (B[‡]) and the coefficient of determination (R^2). A quite reasonable agreement between estimated and measured evaporation rates was obtained at the hourly timescale with a high linear representation ($R^2 = 0.95$).

Fig. 4 shows the diurnal variation of evaporation simulated by the model compared to EC data for eight distinct days. A good agreement is observed between the daily cycle of model estimates and EC measurements in spite of a slight overestimation on 14-Jun-2008 and a minor underestimation at the end of the 2008 season (09-Aug-2008). The strong soil water content depletion during 2007 is evidenced through a significant reduction in λE_t (Figs. 4a-4c), despite the almost constant LAI_f (Fig. 2k). In 2008, the initial growing period (Fig. 4d) is characterized by the low foliage area of the vines ($LAI_f = 0.7$ m^2 m^{-2}), when λE_t emanates mainly from bare and vegetated soils. When vine LAI_f increases, its transpiration increases leading to maximum values of latent heat flux around 250 W m^{-2} (Figs. 4f-4g). During the two periods shown in Figs. 4f and 4g, when vine foliage is fully developed (LAI_f close to 3), the agreement between the two λE_t series is rather good. This period of the growing season can be considered as the most important from an agricultural point of view, given the impact

[‡] $B = \sum_1^n (e_i - m_i)/n$, with e_i the estimated value and m_i the observed value at time step i

of water stress on grape production (Schultz, 1996).

4.3 Seasonal dynamics of water balance

In this section, the evaporation model is coupled with the soil module to jointly simulate the seasonal dynamics of total evaporation (E_t) and soil water content. E_t is obtained from Eq. (4) using the simulated soil water content θ to solve Eq. (20). The water table being fairly deep (down to 4 m) during the simulation period, the impact of capillary rise is considered as negligible and the corresponding module is shutdown. In addition, the iterative approach presented in Section 2.2.3 is used to obtain the net radiation. It yields relatively good estimates, compared to measured values (RMSE = 46 W m^{-2}; results not shown), but with a slight overestimation, maybe explained by a higher load of atmospheric radiation obtained by the scheme detailed in Appendix D, which certainly would have required a local calibration (e.g. Lhomme et al., 2007).

An overall comparison between simulated and observed E_t and θ values for both seasons is shown in Fig. 5a and 5b, respectively. The simulated value of θ is calculated as the weighted mean of the water content of each reservoir. The evaporation results show a relatively good agreement between model and EC data, with a regression slope close to 1, but some overestimation is observed. A possible explanation is the method implemented for estimating net radiation, which led to an overestimation of this input variable (bias = +21 W m^{-2} between 07:00 and 18:00 local time), and therefore an increase of available energy for evaporation. The same comparison for θ (Fig. 5b) shows that very good estimates were obtained for both contrasting seasons.

Fig. 6 shows the time series of modeled daily evaporation and soil water content during the two seasonal simulations. In general, the agreement between the simulated curves and the observed data is rather good. A strong temporal decay in both evaporation and θ characterizes the 2007 season, as a response of very low precipitations (Fig. 2i). For the 2008 season (Fig. 6b), the evaporation experiences a seasonal course that agree quite well with EC measurements. The seasonal evolution follows the seasonal shape of the meteorological forcing and foliage development. Concerning soil water content (θ), a slight increase induced by a relatively low evaporative demand and by several rainfall events (till mid-June 2008, see Fig. 2j) is followed by a progressive decrease until the end of the growing season (Fig. 6d). During the last part of the period (September 2008), overestimated values of θ are obtained with the model, which could receive the following explanation. The dry conditions and the

absence of grass cover during the last part of the growing season have induced soil crusting which reduces the infiltration capacity and enhances surface runoff. Consequently, the strong rainfall event just before the last measurement days (Fig. 2j), which potentially could have involved important water filling for the soil, may have been lost by runoff. This phenomenon was observed by Lebon et al. (2003) in the same region and also by Gaudin et al. (2010) in an inter-cropping vineyard.

4.4 Analysis of model predictions

In order to illustrate model versatility, some static simulations were undertaken in order to examine the SVAT model under different configurations of the vineyard system and to explore the impact of crop characteristics on evaporation.

4.4.1 Impact of capillary rise

A simulation with constant boundary conditions was performed in order to quantify the magnitude of the water flow from the saturated zone into reservoir (3) (CR_3). In our formulation CR_3 varies as a function of the saturated zone depth (z_G) and the soil water content of reservoir (3) (θ_3). The same soil texture (clay loam) for reservoir (3) and the transition zone between z_G and z_R is considered and the corresponding values of hydraulic parameters taken from Clapp and Hornberger (1978) are shown in Table 2. Fig. 7 shows the predicted values of CR_3 as a function of θ_3 and of the distance between the root zone and the water table $z_G - z_R$. As can be anticipated, capillary rise (CR_3 value) decreases with the distance ($z_G - z_R$) and increases with the soil water content θ_3 in relation with the hydraulic conductivity $K_{G,3}$. Although it was not possible to confront these values with field measurements, they are within the range of values obtained by several authors from similar or more complex approaches of capillary rise (e.g. Raes and Deproost, 2003; Bogaart et al. 2008; Vervoort et al. 2008). Our results are realistic and confirm the possible use of the capillary rise module when the water table is shallow.

4.4.2 Impact of vineyard structure on evaporation rate

In our approach, the geometry of the grassed vineyard system can be characterized by the distance between rows and the relative proportion of grass (F_{vs}) and bare soil (F_{bs}). In

order to estimate the impact of foliage surface proportion on vineyard evaporation, the concept of clumped leaf area index ($CLAI_f$) is used (defined as the leaf area per unit area of substrate covered by the foliage): $LAI_f = F_f CLAI_f$, where F_f is the proportion of soil surface occupied by the vine canopy. F_f depends on the width of the vine row (w_r) and on that of the inter-row (w_i), and can be expressed as

$$F_f = \frac{w_r}{w_r + w_i} = \frac{1}{1 + w_i / w_r}. \tag{39}$$

Inter-row width w_i is varied maintaining $CLAI_f$ and w_r fixed: 2.5 and 1 m respectively. In this way, total evaporation is simulated as a function of w_i and hence LAI_f using Eq. (39). Standard values of meteorological and soil variables were considered: R_n = 400 W m^{-2}, T_a = 25 °C, D_a = 10 hPa, u_a = 2 m s^{-1}, R_g = 600 W m^{-2}, θ_f = 0.3, θ_{vs} = 0.25, θ_{bs} = 0.25. Secondly, the proportion of vegetated soil F_{vs} (and consequently F_{bs}) is varied between 0 (bare soil only) and 1 (grassed soil only). The model is run by considering the combined effect of w_i and F_{vs} variations on total evaporation E_t, all other conditions being kept constant. The results of this simulation are shown in Fig. 8: for F_{vs} = 0.3 (our experimental dataset) a decrease in E_t of about 0.02 mm h^{-1} is estimated when the distance between rows w_i varies from 0.5 to 4 m. For w_i = 2 m, E_t increases of about 0.1 mm h^{-1} when passing from fully bare (F_{vs} = 0) to fully grassed soil (F_{vs} = 1.0), suggesting a higher sensitivity to grass cover.

5. Discussion

A quite good performance of the proposed SVAT model was obtained in representing the seasonal water balance. Model estimates of total evaporation are quite good when considering the surface energy balance module alone (Fig. 3), forced with measured net radiation and soil moisture. They are less accurate when considering the coupling between surface energy balance and soil water balance (Fig. 5). This is ascribed to the fact that net radiation and soil moisture are simulated and not measured. Certainly, the parameterization adopted for foliage surface resistance is critical. Indeed, the model was found very sensitive to the stress function f_3 of Eq. (20) involving soil moisture (θ). In addition, the maximum leaf conductance of grapevine $g_{x,f}$ (Eq. (17)) was found to be highly variable in the literature. It might also vary in time as a function of phenological stage and environmental conditions, so

905 that the use of a single value over the whole season might be inappropriate. Previous works
906 have shown that parameter sensitivity can vary for different periods (Demarty et al., 2005;
907 Guillevic et al., 2012) and that a period-specific calibration associated with the seasonal
908 variability in vegetation properties or rainfall should be preferable (Coron et al., 2012;
909 Gharari et al., 2013).

910 The equations used for aerodynamic resistances (Appendix C) are very common in
911 micrometeorology but they could be a source of uncertainty. Indeed, given the influence of
912 vineyard geometry on wind flow within and above the foliage, there is a gap in the current
913 parameterizations of surface aerodynamic properties of crop canopies structured in rows. In
914 this sense, the influence of wind direction and row orientation has been reported in the
915 literature. For the case of vineyards, a significant increase in drag coefficient was found by
916 Hicks (1973) and a larger turbulent intensity by Weiss and Allen (1976) when wind flows
917 perpendicular to the rows. Also, important differences were found by Riou et al. (1987) for
918 vineyard aerodynamic parameters (z_0 and d) as a function of wind direction and row
919 orientation, and variations in measured daytime aerodynamic resistance were found by Padro
920 et al. (1994) for different wind directions likely due to variations in z_0. Recently, using Large
921 Eddy Simulation under neutral conditions, a major channeling effect between the vine rows
922 was described by Chahine et al. (2014) for row-parallel wind, increasing the spatial variability
923 in vertical wind profile and decreasing the value of aerodynamic parameters such as z_0 and d
924 in relation to normal and diagonal flow. They concluded that this effect may be more
925 pronounced under unstable conditions, which might be expected in Mediterranean regions
926 during the growing season. These points raise the challenge of improving the current
927 parameterizations of aerodynamic resistances including wind direction effects.

928 Uncertainties associated with R_n estimates and LAI_f simulations also play an important
929 role on the partition of available energy and on surface and aerodynamic resistances. More
930 complex models than Beer's law can be found in the literature for canopy radiative transfer
931 (Taconet et al., 1986; Braud et al., 1995). Lebon et al. (2003) stressed that a better partitioning
932 of incoming solar radiation between vines and substrate is obtained by using the model of
933 Riou et al. (1989) which involves vineyard geometrical properties. This model, only designed
934 for shortwave radiation, was later developed by Pieri (2010a, 2010b) for long-wave radiation
935 partitioning. For the specific case of row-growing crops, a comprehensive model for radiative
936 transfer and partition (short- and long-wave radiation) was recently proposed by Colaizzi et al.
937 (2012a, 2012b). Unfortunately, given the data requirements of these radiative models, their
938 implementation is rather difficult considering the scope of the present work.

A better representation of water stress and its impact on gas exchanges might be addressed by taking into account the mechanisms responsible for variations in soil water distribution and root water uptake along the profile (e.g. Tuzet et al., 2003; Amenu and Kumar, 2008; Siqueira et al., 2008; Volpe et al., 2013). Certainly the simplified approach adopted here represents a source of uncertainty to the model, especially in relation with vine roots depth, their distribution and their impacts on soil moisture dynamics. However, the inclusion of soil profiles into the soil water balance module would have significantly altered the parsimonious nature of the model, and therefore its possible use at the regional extent.

Finally, it is clear that assuming a complete infiltration of rainfall can lead to some discrepancies between model outputs and observations after strong rainfall events, such as the one registered at the beginning of September 2008 (Figs. 2j, 6d). But the inclusion of runoff into the soil water budget is a quite complex issue to solve in a one-dimensional approach. The improvement of this component requires considering the horizontal heterogeneities in soil physical properties responsible for horizontal transfers and could be carried out by coupling SVAT models with spatially-distributed hydrological models (e.g. Bouilloud et al. 2010).

6. Concluding remarks

In this work, the seasonal pattern of evaporation from a grassed Mediterranean vineyard was modeled by coupling an evaporation formulation together with a reservoir-type soil water balance model. The evaporation formulation is based on a three-source model, recently revisited by Lhomme et al. (2012), where some adaptations have been made in order to use standard meteorological data as direct inputs to the model. This approach provides realistic estimates of the component evaporations emanating from the three sources (main foliage, grassed and bare soil) and allows the seasonal dynamics of soil moisture to be correctly simulated. A good agreement was obtained when the seasonal course of total evaporation and soil moisture simulations were compared against ground based references during two contrasting seasons in terms of available soil water. Neglecting runoff, however, can lead to some discrepancy after strong rainfall events on dry soil: soil crusting promotes runoff and lower soil moisture recharge. This imposes limitations to the application of the model and further investigation should focus on the coupling with distributed hydrological models.

The model versatility can be used to explore the impact of the grassed vineyard

geometry on evaporation throughout the season and for different climate conditions. The static simulations performed suggest that a significant impact should be expected when the distance between vine rows and the fraction of grassed soil are modified.

Apart from the aforementioned limitations regarding the model performance, uncertainties arise from the fact that a large number of parameters should be defined for the controlling factors. This difficulty has been addressed by applying an optimization procedure to find the optimal values of these parameters. However, these values can vary in relation with grapevine phenological phases and could be improved by testing a larger number of model outputs against measurements of energy and water balance.

Finally, another contribution of this parsimonious model is its potential use to estimate water budget components at regional scale using remotely sensed data. The energy balance-based evaporation formulation allows one to derive surface composite temperature which can be compared to the satellite estimate of the corresponding radiometric temperature. Different approaches have been developed to include this temperature into SVAT models through data assimilation schemes in order to obtain energy balance components (Coudert et al., 2006; Caparrini et al. 2008; Sini et al., 2008) or soil moisture estimates (Jones et al., 1998; Crow et al., 2008).

Acknowledgements

This study was partly supported by the French Centre National d'Etudes Spatiales (CNES/TOSCA) and by the European Commission's Seventh Framework Programme (FP7/2007-2013) through the 'Research Infrastructures' action under ExpeER project (grant agreement n°262060). The first author acknowledges CONICYT-Chile for the doctoral grant. The constructive comments and suggestions from three anonymous reviewers are highly appreciated.

Appendix A. Coefficients of the evaporation formulation (Eq. (4))

$$P_f = r_a R_{vs} R_{bs} / DE, \tag{A1}$$

$$P_{vs} = r_a R_f R_{bs} / DE, \tag{A2}$$

$$P_{bs} = r_a R_f R_{vs} / DE, \tag{A3}$$

with DE written as

$$DE = R_f R_{vs} R_{bs} + R_f R_{vs} R_a + R_f R_{bs} R_a + R_{vs} R_{bs} R_a, \tag{A4}$$

with the coefficients R_i being defined as

$$R_f = r_{s,f} + \left(n + \frac{\Delta}{\gamma} \right) r_{a,f,h}, \tag{A5}$$

$$R_{vs} = r_{s,vs} + \left(1 + \frac{\Delta}{\gamma} \right) r_{a,vs}, \tag{A6}$$

$$R_{bs} = r_{s,bs} + \left(1 + \frac{\Delta}{\gamma} \right) r_{a,bs}, \tag{A7}$$

$$R_a = r_a \left(1 + \frac{\Delta}{\gamma} \right). \tag{A8}$$

Appendix B: Expressing the component surface temperatures

Component surface temperatures T_i ($i = f$, vs, bs) are obtained by solving the energy balance for the three sources. The corresponding available energy (A_i) is equal to the sum of

latent and sensible heat fluxes:

$$A_i = \frac{\rho c_p}{\gamma} \frac{\left[e^*(T_i) - e_m\right]}{r_{s,i} + r_{a,i,v}} + \rho c_p \frac{T_i - T_m}{r_{a,i,h}}, \tag{B1}$$

$r_{a,i,v}$ and $r_{a,i,h}$ representing the air resistances respectively for water vapor and sensible heat, T_m and e_m the air temperature and air vapor pressure at canopy source height (z_m), and $e^*(T_i)$ the saturated vapor pressure at T_i. After linearizing $e^*(T_i) - e^*(T_m)$, Eq. (B1) is rewritten as:

$$A_i = \frac{\rho c_p}{\gamma} \frac{\left[\Delta(T_i - T_m) + D_m\right]}{r_{s,i} + r_{a,i,v}} + \rho c_p \frac{T_i - T_m}{r_{a,i,h}}. \tag{B2}$$

After some algebra and taking into account that $r_{a,i,v} = n\, r_{a,i,h}$, surface temperature can be expressed as:

$$T_i - T_m = \frac{\left(n r_{a,i,h} + r_{s,i}\right) A_i / \rho c_p - D_m / \gamma}{n + \Delta/\gamma + r_{s,i} / r_{a,i,h}}, \tag{B3}$$

with $n = 2$ for the foliage ($i = f$) and $n = 1$ for the substrate components ($i = vs, bs$), T_m being obtained by $T_m = T_a + H\, r_a / \rho c_p$.

Appendix C: Formulations of aerodynamic resistances

The aerodynamic resistance above the canopy (r_a) is calculated using the equation that takes into account the stability correction functions for wind (Ψ_m) and temperature (Ψ_h) (Brutsaert, 1982):

$$r_a = \left(\frac{1}{k^2 u_a}\right)\left[\ln\left(\frac{z_r - d}{z_0}\right) - \Psi_h\left(\frac{z_r}{L}\right)\right]\left[\ln\left(\frac{z_r - d}{z_0}\right) - \Psi_m\left(\frac{z_r}{L}\right)\right], \tag{C1}$$

where u_a is the wind speed at reference height z_r and L is the Monin-Obukhov length. The

canopy roughness length z_0 is determined following Choudhury and Monteith (1988):

$$z_0 = \begin{cases} \bar{z}_{0,s} + 0.3 z_h X^{0.5}, & \text{if } 0 < X \le 0.2 \\ 0.3 z_h \left(1 - \dfrac{d}{z_h}\right), & \text{if } 0.2 < X < 1.5 \end{cases} \tag{C2}$$

where $X = c_d LAI_f$, with c_d = 0.2 the mean drag coefficient assumed to be uniform within the canopy and $\bar{z}_{0,s}$ the average value of substrate roughness length (= 0.0125 m). Following the same authors the displacement height d is expressed by

$$d = 1.1 z_h \ln\left(1 + X^{0.25}\right), \tag{C3}$$

where z_h is the mean canopy height (vineyard).

The aerodynamic resistance between the substrate (i = vs and bs) and the canopy source height (d + z_0) is calculated (per unit area of substrate) as (Choudhury and Monteith, 1988)

$$r_{a,i}^{1} = \frac{z_h \exp(\alpha_w)}{\alpha_w K(z_h)} \left\{ \exp\left[-\alpha_w z_{0,i}/z_h\right] - \exp\left[-\alpha_w (d + z_0)/z_h\right] \right\}, \tag{C4}$$

where z_h is the height of the main foliage (vineyard), α_w = 2.5 (dimensionless), $z_{0,i}$ the roughness length for momentum of vegetated ($z_{0,vs}$ = 0.015 m) and bare soil ($z_{0,bs}$ = 0.010 m). $K(z_h)$ is the value of eddy diffusivity at canopy height, obtained by

$$K(z_h) = \frac{k^2 u_a (z_h - d)}{\ln\left[(z_r - d)/z_0\right]}. \tag{C5}$$

Foliage bulk boundary later resistance for sensible heat is expressed as (Choudhury and Monteith, 1988)

$$r_{a,f,h} = \frac{\alpha_w \left[w/u(z_h)\right]^{1/2}}{4\alpha_0 LAI_f \left[1 - \exp(-\alpha_w/2)\right]}, \tag{C6}$$

where w is leaf width (0.01 m), α_0 is a constant equal to 0.005 (in m $s^{-1/2}$) and $u(z_h)$ is the wind speed at z_h, obtained by

$$u(z_h) = u_a \frac{\ln\left[(z_h - d)/z_0\right]}{\ln\left[(z_r - d)/z_0\right]}. \tag{C7}$$

Appendix D: Estimating atmospheric radiation

The incoming longwave radiation (R_{atm}) was parameterized using a formulation including both the effects of clear and cloudy sky conditions on R_{atm}. Several methods have been developed to estimate this component of radiative budget, which are often based on empirical formulations depending on air temperature and humidity (e.g. Brunt, 1932; Idso and Jackson, 1969; Duarte et al., 2006). In the present study the Brutsaert (1975) formulation was used to calculate the clear sky atmospheric radiation which is expressed as

$$R_{atm,c} = a_1 (e_a / T_a)^{b_1} \sigma T_a^4, \tag{D1}$$

e_a is the actual vapor pressure (Pa), and a_1 and b_1 are constant with values 1.24 and 0.14, respectively. Under cloudy sky conditions the fractional cover should be used, but this measure is very difficult to obtain in operational terms using conventional weather stations. Crawford and Duchon (1999) showed that a good estimation of sky condition could be obtained using the ratio R_g / R_0 between the measured solar irradiance (R_g) and the clear-sky irradiance (R_0). R_0 was obtained as a fraction of the extraterrestrial radiation (R_{ext}, the theoretical solar radiation at the top of the atmosphere) using the formulation proposed by Allen et al. (1998):

$$R_0 = R_{ext}\left(0.75 + 2 \times 10^{-5} Z\right), \tag{D2}$$

with Z the site elevation (masl). So, considering both clear and cloudy skies conditions the downwelling longwave atmospheric radiation is estimated as (Crawford and Duchon, 1999)

$$R_{atm} = R_{atm,c}(R_g / R_0) + \left(1 - R_g / R_0\right)\sigma T_a^4. \quad \text{(D3)}$$

Since during nighttime the ratio R_g / R_0 cannot be calculated, Eq. (D3) was computed using the last value of R_g / R_0 during the previous afternoon (e.g. Lhomme et al., 2007).

References

Allen, R.G., Jensen, M.E., Wright, J.L., Burman, R.D., 1989. Operational estimates of reference evapotranspiration. Agron. J. 81,650-662.

Allen, R.G., Pereira, L.S., Raes, D., Smith, M., 1998. Crop evapotranspiration. FAO Irrigation and Drainage Paper 56, Rome.

Amenu, G.G., Kumar, P., 2008. A model for hydraulic redistribution incorporating coupled soil-root moisture transport. Hydrol. Earth Syst. Sci. 12, 55-74.

Anderson, M.A., Norman, J.M., Diak, G.R., Kustas, W.P., Mecikalski, J.R., 1997. A two-source time-integrated model for estimating surface fluxes using thermal infrared remote sensing. Remote Sens. Environ. 60, 195-216.

Anderson, M.C., Norman, J.M., Kustas, W.P., Li, F., Prueger, J.H., Mecikalski, J.R., 2005. Effects of vegetation clumping on two-source model estimates of surface energy fluxes from an agricultural landscape during SMACEX. J. Hydrometeorol. 6, 892-909.

Bastidas, L.A., Gupta, H.V., Sorooshian, S., Shuttleworth, W.J., Yang, Z.L., 1999. Sensitivity analysis of a land surface scheme using multicriteria methods. J. Geophys. Res. 104, 19481– 19490.

Bogaart, P.W., Teuling, A.J., Troch, P.A., 2008. A state-dependent parameterization of saturated-unsaturated zone interaction. Water Resour. Res. 44, 1-10.

Bouilloud, L., Chancibault, K., Vincendon, B., Ducrocq, V., Habets, F., Saulnier, G.-M., Anquetin, S., Martin, E., Noilhan, J., 2010. Coupling the ISBA land surface model and the TOPMODEL hydrological model for Mediterranean flash-flood forecasting: description, calibration, and validation. J. Hydrometeorol. 11, 315-333.

Boulet, G., Chehbouni, G., Braud, I., Vauclin, M., 1999. Mosaic versus dual source approaches for modelling the surface energy balance of a semi-arid land. Hydrol. Earth Syst. Sci. 3, 247-258.

Boulet, G., Chehbouni, A., Braud, I., Vauclin, M., Haverkamp, R., Zammit, C., 2000. A simple water and energy balance model designed for regionalization and remote sensing data utilization. Agr. Forest Meteorol. 105, 117-132.

Braud, A.C., Dantas-Antonino, M., Vauclin, J.L., Thony, Ruelle, P., 1995. A simple soil-plant-atmosphere transfer model (SiSPAT) development and field verification. J. Hydrol. 166, 213-250.

Brenner, A.J., Incoll, L.D., 1997. The effect of clumping and stomatal response on evaporation from sparsely vegetated shrublands. Agr. Forest Meteorol. 84, 87-205.

Brunt, D., 1932. Notes on radiation in the atmosphere. Q. J. Roy. Meteor. Soc. 58, 389-420.

Brutsaert,W.H., 1975. On a derivable formula for long-wave radiation from clear skies. Water Resour. Res. 11, 742-744.

Brutsaert, W., 1982. Evaporation into the Atmosphere. Reidel Publishing Company, Dordrecht, 299 pp.

Campbell, G.S., 1974. A simple method for determining unsaturated hydraulic conductivity from moisture retention data. Soil Sci. 177, 311-314.

Caparrini, F., Castelli, F., Entekhabi, D., 2004. Estimation of surface turbulent fluxes through assimilation of radiometric surface temperature sequences . J. Hydrometeorol. 5, 145-159.

Celette, F., Wery, J., Chantelot, E., Celette, J., Gary, C., 2005. Belowground interactions in a vine (Vitis vinifera L.)-tall fescue (*Festuca arundinacea* Shreb.) intercropping system: water relations and growth. Plant Soil. 276, 205-217.

Celette, F., Gaudin, R., Gary, C., 2008. Spatial and temporal changes to the water regime of a Mediterranean vineyard due to the adoption of cover cropping. Eur. J. Agron. 29, 153-162.

Celette, F., Ripoche, A., Gary, C., 2010. WaLIS – A simple model to simulate water partitioning in a crop association: The example of an intercropped vineyard. Agr. Water Manage. 97, 1749-1759.

Centinari, M., Poni, S., Intrigliolo, D.S., Dragoni, D., Lakso, A.N., 2012. Cover crop evapotranspiration in a northeastern US Concord (*Vitis labruscana*) vineyard. Aust. J. Grape Wine Res. 18, 73-79.

Chahine, A., Dupont, S., Sinfort, C., Brunet, Y., 2014. Wind-flow dynamics over vineyards. Bound.-Lay. Meteorol. DOI 10.1007/s10546-013-9900-4

Choudhury, B.J., Monteith, J.L., 1988. A four-layer model for the heat budget of homogeneous land surfaces. Q. J. Roy. Meteor. Soc. 114, 373-398.

Choudhury, B.J., 1989. Estimating evaporation and carbon assimilation using infrared temperature data: vistas in modeling. In G. Asrar (ed.), Theory and applications of optical remote sensing. Wiley, New York.

Choudhury, B.J., Idso, S.B., Reginato, R.G., 1987. Analysis of an empirical model for soil heat flux under a growing wheat crop for estimating evaporation by an infrared-temperature based energy balance equation. Agr. Forest Meteorol. 39, 283-297.

Clapp, R.B., Hornberger, G.M., 1978. Empirical equations for some soil hydraulic properties. Water Resour. Res. 14, 601-604.

Clevers, J.G.P.W., Vonder, O.W., Jongschaap, R.E.E., Desprats, J., King, C., Prévot, L., Ruguier, N., 2002. Using SPOT data for calibrating a wheat growth model under

mediterranean conditions. Agronomie 22, 687-694.

Colaizzi, P.D., Evett, S.R., Howell, T.A., Li, F., Kustas, W.P., Anderson, M.C., 2012a. Radiation model for row crops: I. Geometric view factors and parameter optimization. Agron. J. 104, 225-240.

Colaizzi, P.D., Scwartz, R.C., Evett, S.R., Howell, T.A., Gowda, P.H., Tolk, J.A., 2012b. Radiation model for row crops: II. Model evaluation. Agron. J. 104, 241-255.

Coron, L., Andréassian, V., Perrin, C., Lerat, J., Vaze, J., Bourqui, M., Hendrickx, F., 2012. Crash testing hydrological models in contrasted climate conditions: An experiment on 216 Australian catchments. Water Resour. Res. 48, W05552, doi:10.1029/2011WR011721

Coudert, B., Ottlé, C., Boudevillain, B., Demarty, J., Guillevic, P., 2006. Contribution of thermal infrared remote sensing data in multiobjective calibration of a dual-source SVAT model . J. Hydrometeorol. 7, 404-420.

Crawford, T.M., Duchon, C.E., 1999. An improved parameterization for estimating effective atmospheric emissivity for use in calculating daytime downwelling longwave radiation. J. Appl. Meteorol. 38, 474-480.

Crow, W.T., Kustas, W.P., Prueger, J.H., 2008. Monitoring root-zone soil moisture through the assimilation of a thermal remote sensing-based soil moisture proxy into a water balance model. Remote Sens. Environ. 112, 1268-1281.

Davies, J.A., 2006. A note on the relationship between net radiation and solar radiation. Q. J. Roy. Meteor. Soc. 93, 109-115.

Demarty, J., Ottlé, C., Braud, I., Olioso, A., Frangi, J.P., Bastidas, L.A., Gupta, H.V., 2004. Using a multiobjective approach to retrieve information on surface properties used in a SVAT model. J. Hydrol. 287, 214-236.

Demarty, J., Ottlé, C., Braud, I., Olioso, A., Frangi, J.P., Gupta, H.V., Bastidas, L.A., 2005. Constraining a physically based Soil-Vegetation-Atmosphere Transfer model with surface water content and thermal infrared brightness temperature measurements using a multiobjective approach. Water Resour. Res. 41, W01011, doi:10.1029/2004WR003695.

Duarte, H.F., Dias, N.L., Maggiotto, S.R., 2006. Assessing daytime downward long-wave radiation estimates for clear and cloudy skies in Southern Brazil. Agr. Forest Meteorol. 139, 171-181.

Fisher, J.I., Mustard, J.F., Vadeboncoeur M.A., 2006. Green leaf phenology at Landsat resolution: scaling from the field to the satellite. Remote Sens. Environ. 100, 265-279.

Galleguillos, M., Jacob, F., Prévot, L., French, A., Lagacherie, P., 2011. Comparison of two

temperature differencing methods to estimate daily evapotranspiration over a Mediterranean vineyard watershed from ASTER data. Remote Sens. Environ. 115, 1326-1340.

Gaudin, R., Celette, F., Gary, C., 2010. Contribution of runoff to incomplete off season soil water refilling in a Mediterranean vineyard. Agr. Water Manage. 97, 1534-1540.

Gharari, S., Hrachowitz, M., Fenicia, F., Savenije, H.H.G., 2013. An approach to identify time consistent model parameters: sub-period calibration. Hydrol. Earth Syst. Sci. 17, 149-161.

Graser, E.A., Van Babel, C.H.M., 1982. The effect of soil moisture upon soil albedo. Agr. Meteorol. 27, 17-26.

Guillevic, P.C., Privette, J.L., Coudert, B., Palecki, M.A., Demarty, J., Ottlé, C., Augustine, J.A., 2012. Land Surface Temperature product validation using NOAA's surface climate observation networks - scaling methodology for the Visible Infrared Imager Radiometer Suite (VIIRS). Remote Sens. Environ. 124, 282-298.

Guix-Hébrard, N., Voltz, A., Trambouze, W., Garnier, F., Gaudillère, J.P., Lagacherie, P., 2007. Influence of watertable depths on the variation of grapevine water status at the landscape scale. Eur. J. Agron. 27, 187-196.

Gupta, H.V., Bastidas, L.A., Sorooshian, S., Shuttleworth, W.J., Yang, Z.L., 1999. Parameter estimation of a land surface scheme using multicriteria methods. J. Geophys. Res. 104, 19491-19503.

Hicks, B.B., 1973. Eddy flux over a vineyard. Agric. For. Meteorol. 12, 203-215.

Holland, S., Heitman, J.L., Howard, A., Sauer, T.J., Giese, W., Ben-Gal, A., Agam, N., Kool, D., Havlin, J., 2013. Micro-Bowen ratio system for measuring evapotranspiration in a vineyard interrow. Agric. Forest Meteorol. 177, 93-100.

Idso, S.B., Jackson, R.D., 1969. Thermal radiation from the atmosphere. J. Geophys. Res. 74, 5397-5403.

Idso, S.B., Jackson, R.D., Reginato, R.J., Kimball, B.A., Nakayama, F.S., 1975. The dependence of bare soil albedo on soil water content. J. Appl. Meteorol. 14, 109-113.

Jarvis, P.G., 1976. The interpretation of leaf water potential and stomatal conductance found in canopies in the field. Phil. Trans. Roy. Soc. Lond. B. 273, 593-610.

Jones, A.S., Guch, I.C., Vonder Haar, T.H., 1998. Data assimilation of satellite-derived heating rates as proxy surface wetness data into a regional atmospheric mesoscale model. Part I: Methodology . Mon. Wea. Rev. 126, 634-645.

Jones, H.G., Stoll, M., Santos, T., de Sousa, C., Chaves, M.M., Grant, O.M., 2002. Use of

infrared thermography for monitoring stomatal closure in the field: application to grapevine. J. Exp. Bot. 53 (378), 2249-2260.

Kustas, W.P., Zhan, X., Schmugge, T.J., 1998. Combining optical and microwave remote sensing for mapping energy fluxes in a semiarid watershed. Remote Sens. Environ. 64, 116-131.

Lebon, E., Dumas, V., Pieri, P., Schultz, H.R., 2003. Modelling the seasonal dynamics of the soil water balance of vineyards. Funct. Plant Biol. 30, 699-710.

Lhomme, J.P., Chehbouni, A., 1999. Comments on dual-source vegetation–atmosphere transfer models. Agr. Forest Meteorol. 94, 269-273.

Lhomme, J.P., Monteny, B., 2000. Theoretical relationship between stomatal resistance and surface temperatures in sparse vegetation. Agr. Forest Meteorol. 104, 119-131.

Lhomme, J.P., Vacher, J.J., Rocheteau, A., 2007. Estimating downward long-wave radiation on the Andean Altiplano. Agr. Forest Meteorol. 145, 139-148.

Lhomme, J.P., Montes, C., Jacob, F., Prévot, L., 2012. Evaporation from heterogeneous and sparse canopies: on the formulations related to multi-source representations. Bound.-Lay. Meteorol. 144, 243-262.

Mahfouf, J.-F., and J. Noilhan, 1991. Comparative study of various formulations of evaporation from bare soil using in-situ data. J. Appl. Meteorol., 30, 1354-1365.

Maxwell, R.M., Miller, N.L., 2005. Development of a coupled land surface and groundwater model. J. Hydrometeorol. 6, 233-247.

Monteith, J.L., 1965. Evaporation and the environment, in: The state and movement of water in living organisms, XIX symposium, Soc. Exp. Biol., Swansea, Cambridge University Press, 205:234.

Morlat, R., Jacquet A., 2003. Grapevine root system and soil characteristics in a vineyard maintained long-term with or without interrow sward. Am. J. Enol. Vitic. 54, 1-7.

Moussa, R., Chahinian, N., Bocquillon, C., 2007. Distributed hydrological modelling of a Mediterranean mountainous catchment — Model construction and multi-site validation. J. Hydrol. 337, 35-51.

Norman, J.M., Kustas, W.P., Humes, K.S., 1995. Source approach for estimating soil and vegetation energy fluxes in observations of directional radiometric surface temperature. Agr. Forest Meteorol. 77, 263-293.

Ortega-Farias, S., Carrasco, M., Olioso, A., Acevedo, C., Poblete, C., 2007. Latent heat flux over Cabernet Sauvignon vineyard using the Shuttleworth and Wallace model. Irrigation Sci. 25, 161–170.

Ortega-Farias, S., Poblete-Echeverría, C., Brisson, N., 2010. Parameterization of a two-layer model for estimating vineyard evapotranspiration using meteorological measurements. Agr. Forest Meteorol. 150, 276-286.

Padro, J., Massman, W.J., Den Hartog, G., Neumann, H.H., 1994. Dry deposition velocity of O_3 over a vineyard obtained from models and observations: The 1991 California ozone deposition experiment. Water Air Soil Pollut. 75, 307-323.

Paré, N., 2011. Construction d'un modèle couplé pression-impact pour l'expérimentation virtuelle de pratiques culturales à l'échelle de petits bassins versants. PhD Thesis, Montpellier SupAgro. Montpellier, France. 300p.

Pellegrino, A., Lebon, E., Simonneau, T.M., Wery, J., 2005. Towards a simple indicator of water stress in grapevine (*Vitis vinifera* L.) based on the differential sensitivities of vegetative growth components. Aust. J. Grape Wine Res. 11, 306-315.

Pieri, P., 2010a. Modelling radiative balance in a row-crop canopy: Cross-row distribution of net radiation at the soil surface and energy available to clusters in a vineyard. Ecol. Model. 221, 802-811.

Pieri, P., 2010b. Modelling radiative balance in a row-crop canopy: Row–soil surface net radiation partition. Ecol. Model. 221, 791-801.

Pieri, P., Gaudillère, J.P., 2003. Sensitivity to training system parameters and soil surface albedo of radiation intercepted by vine rows. Vitis. 42, 77-82.

Poblete-Echeverria, C., Ortega-Farias, S., 2009. Estimation of actual evapotranspiration for a drip-irrigated Merlot vineyard using a three-source model. Irrigation Sci. 28, 65-78.

Pradel, C., Pieri, P., 2000. Influence of a grass layer on vineyard soil temperature. Aust. J. Grape Wine Res. 6, 59-67.

Raes, D., Deproost, P., 2003. Model to assess water movement from a shallow water table to the root zone. Agr. Water Manage. 62, 79-91.

Rana, G., Katerji, N., 2008. Direct and indirect methods to simulate the actual evapotranspiration of an irrigated overhead table grape vineyard under Mediterranean conditions. Hydrol. Process. 22, 181-188.

Raupach, M.R., 1989. A practical Lagrangian method for relating scalar concentrations to source distributions in vegetation canopies. Q. J. Roy. Meteorol. Soc. 115, 609-632.

Riou, C., Pieri, P., Valancogne, C., 1987. Variation de la vitesse du vent a l'intérieur et au-dessus d'une vigne. Agr. Forest Meteorol. 39, 143-154.

Riou, C., Valancogne, C., Pieri, P., 1989. Un modèle simple d'interception du rayonnement solaire par la vigne - Vérification expérimentale. Agronomie. 9, 441–450.

Riou, C., Pieri, P., Le Clech, B., 1994. Consommation d'eau de la vigne en conditions hydriques non limitantes. Formulation simplifies de la transpiration. Vitis. 33, 109-115.

Rodriguez-Iturbe, I., 2000. Ecohydrology: A hydrologic perspective of climate-soil-vegetation dynamics. Water Resour. Res. 36, 3-9.

Saux-Picart, S., Ottlé, C., Perrier, A., Decharme, B., Coudert, B., Zribi, M., Boulain, N., Cappelaere, B., Ramier, D., 2009. SEtHyS_Savannah: A multiple source land surface model applied to Sahelian landscapes. Agr. Forest Meteorol. 149, 1421-1432.

Schultz, H.R., 1996. Water relations and photosynthetic response of two grapevine cultivars of different geographical origin during water stress. Acta Hortic. 427, 251-266.

Sene, K.J., 1994. Parameterisations for energy transfers from a sparse vine crop. Agr. Forest Meteorol. 71, 1-18.

Sene, K.J., 1996. Meteorological estimates for the water balance of a sparse vine crop growing in semiarid conditions. J. Hydrol. 179, 259-280.

Sellers, P.J., Heiser, M.D., Hall, F.G., 1992. Relations between surface conductance and spectral vegetation indices at intermediate (100 m^2 to 15 km^2) length scales. J. Geophys. Res. 97, 19033–19059.

Shuttleworth, W.J., Wallace, J.S., 1985. Evaporation from sparse crops - an energy combination theory. Q. J. Roy. Meteor. Soc. 111, 839-855.

Shuttleworth, W.J., Gurney, R.J., 1990. The theoretical relationship between foliage temperature and canopy resistance in sparse crops. Q. J. Roy. Meteor. Soc. 111, 839-855.

Sini, F., Boni, G., Caparrini, F., Entekhabi, D., 2008. Estimation of large-scale evaporation fields based on assimilation of remotely sensed land temperature . Water. Resour. Res. 44, W06410, doi:10.1029/2006WR005574 .

Siqueira, M., Katul, G., Porporato, A., 2008. Onset of water stress, hysteresis in plant conductance, and hydraulic lift: Scaling soil water dynamics from millimeters to meters. 44, W01432, doi:10.1029/2007WR006094.

Soylu, M.E., Istanbulluoglu, E., Lenters, J.D., Wang, T., 2011. Quantifying the impact of groundwater depth on evapotranspiration in a semi-arid grassland region. Hydrol. Earth Syst. Sci. 15, 787-806.

Spano, D., Snyder, R.L., Sirca, C., Duce, P., 2009. ECOWAT – A model for ecosystem evapotranspiration estimation. Agr. Forest Meteorol. 149, 1584-1596.

Stewart, J.B., 1988. Modelling surface conductance of pine forest. Agr. Forest. Meteorol. 43, 19-35.

Taconet, O., Bernard, R., Vidal-Madjar, D., 1986. Evapotranspiration over an agricultural

region using a surface flux/temperature model based on NOAA-AVHRR data. J. Clim. Appl. Meteorol. 25, 284-307.

Trambouze, W., Bertuzzi, P., Voltz, M., 1998. Comparison of methods for estimating actual evapotranspiration in a row-cropped vineyard. Agr. Forest Meteorol. 91, 193-208.

Trambouze, W., Voltz, M., 2001. Measurement and modelling of the transpiration of a Meditarranean vineyard. Agr. Forest Meteorol. 107, 153-166.

Tuzet, A., Perrier, A., Leuning, R., 2003. A coupled model of stomatal conductance, photosynthesis and transpiration. Plant Cell Environ. 26, 1097-1116.

Van den Hurk, B.J.J.M., McNaughton, K.G., 1995. Implementation of near-field dispersion in a simple two-layer surface resistance model. J. Hydrol. 166, 293-311.

Vaudour, E., 2003. Les terroirs viticoles. Dunod, Paris, 312p.

Verhoef, A., Allen, S.J., 2000. A SVAT scheme describing energy and CO_2 fluxes for multi-component vegetation: calibration and test for a Sahelian savannah. Ecol. Model. 127, 245-267.

Vervoort, R.W., van der Zee, S.E.A.T.M., 2008. Simulating the effect of capillary flux on the soil water balance in a stochastic ecohydrological framework. Water Resour. Res. 44, W08425, doi:10.1029/2008WR006889.

Volpe, V., Marani, M., Albertson, J.D., Katul, G., 2013. Root controls on water redistribution and carbon uptake in the soil–plant system under current and future climate. Adv. Water Resour. 60, 110-120.

Weiss, A., Allen, L.H.J., 1976. Air flow patterns in vineyard rows. Agric. Meteorol. 16, 329-342.

Winkel, T., Rambal, S., 1990. Stomatal conductance of some grapevines growing in the field under Mediterranean environment. Agr. Forest Meteorol. 51, 107-121.

Winkler, A.J., Williams, W.O., 1939. The hear required to bring Tokay grapes to maturity. Proceedings of the American Society of Horticultural Science. 37, 650-652.

Wu, A., Black, A., Verseghy, D.L., Bailey, W.G., 2001. Comparison of two-layer and single-layer canopy models with Lagrangian and *K*-theory approaches in modeling evaporation from forests. Int. J. Climatol. 21, 1821-1839.

Yi, C. 2008. Momentum transfer within canopies, J. Appl. Meteorol. Climatol. 47, 262-275.

Zhang, B.Z., Kang, S.Z., Li, F.S., Zhang, L., 2008. Comparison of three evapotranspiration models to Bowen ratio-energy balance method for a vineyard in a desert region of northwest China. Agr. Forest Meteorol. 148, 1629-1640.

Zhang , Y.-K., Schilling, K.E., 2006. Effects of land cover on water table, soil moisture

evapotranspiration, and groundwater recharge: A field observation and analysis. J. Hydrol. 319, 328-338.

Zhang, B., Kang, S., Zhang, L., Tong, L., Du, T., 2009. An evapotranspiration model for sparsely vegetated canopies under partial root-zone irrigation. Agr. Forest Meteorol. 149, 2007-2011.

Table 1. Uncertainty range and final values for the fitted parameters of the plant-atmosphere model, as obtained from the MCIP calibration.

Parameter	Equation	Description (units)	Initial uncertainty range	Final calibrated value
Biophysical parameters				
c	7 and 15	Extinction coefficient of main foliage (-)	0.3 – 0.7	0.45
β_{vs}	9	Soil heat flux fraction for vegetated soil (-)	0.1 – 0.4	0.28
β_{bs}	10	Soil heat flux fraction for bare soil (-)	0.2 – 0.5	0.38
$g_{x,f}$	17	Maximal stomatal conductance (main foliage) (m s^{-1})	$1.25\text{x}10^{-3}$ – $1.2\text{x}10^{-2}$	$3.3\text{x}10^{-3}$
$g_{x,vs}$	17	Maximal stomatal conductance (vegetated soil) (m s^{-1})	$3.3\text{x}10^{-3}$ – $1.0\text{x}10^{-2}$	$3.7\text{x}10^{-3}$
a_f	16	Foliage albedo (-)	0.1 – 0.4	0.24
a_{bs}	16	Bare soil albedo (-)	0.2 – 0.5	0.3
a_{vs}	16	Grass albedo (-)	0.15 – 0.35	0.25
Empirical parameters				
K_1^f	18	Parameter of PAR stress function (main foliage) (μmol m^{-2} s^{-1})	80 – 200	150
K_1^{vs}	18	Parameter of PAR stress function (vegetated soil) (W m^{-2})	80 – 140	112
K_2^f	19	Parameter of D_a stress function (main foliage) (kPa^{-1})	$1.575\text{x}10^{-4}$ – $3.125\text{x}10^{-4}$	$2.0\text{x}10^{-4}$
K_2^{vs}	19	Parameter of D_a stress function (vegetated soil) (kPa^{-1})	$3.5\text{x}10^{-2}$ – $1.05\text{x}10^{-1}$	$7.0\text{x}10^{-2}$
K_3^f	20	Parameter of θ stress function (main foliage) (-)	10 – 100	35
K_3^{vs}	20	Parameter of θ stress function (vegetated soil) (-)	10 – 100	45
A_1	21	Parameter of bare soil resistance (-)	5 – 15	8
B_1	21	Parameter of bare soil resistance (-)	1 – 10	5

Table 2. Measured and estimated values of parameters used in the soil water balance model.

Soil parameter	Value	Units	Informative source
Soil profile description			
$\theta_{n,1}$	0.05	$m^3\ m^{-3}$	Trambouze and Voltz, 2001
$\theta_{n,2} = \theta_{n,3} = \theta_{f,wp}$	0.15	$m^3\ m^{-3}$	Trambouze and Voltz, 2001
$\theta_{fc,1}$	0.246	$m^3\ m^{-3}$	*Measured*
$\theta_{fc,2}$	0.268	$m^3\ m^{-3}$	*Measured*
$\theta_{fc,3}$	0.331	$m^3\ m^{-3}$	*Measured*
p_1	0.16	Fraction	*Measured*
p_2	0.20	Fraction	*Measured*
p_3	0.16	Fraction	*Measured*
Capillary rise equations			
$\Psi_{s,3}$	0.63	m	Clapp and Hornberger (1978)
Ψ_G	0.63	m	Clapp and Hornberger (1978)
$\theta_{s,3}$	0.476	$m^3\ m^{-3}$	Clapp and Hornberger (1978)
$K_{s,3}$	2.45×10^{-6}	$m\ s^{-1}$	Clapp and Hornberger (1978)
b_3	8.52	-	Clapp and Hornberger (1978)
Reservoirs depth			
z_1	0.05	m	*Locally estimated*
z_2	0.50	m	*Locally estimated*
z_R	2.0	m	*Locally estimated*

Fig. 1. Schematic representation of the three-source evaporation model and the soil water transfer model. $r_{a,f}$ is the bulk boundary-layer resistance of the main foliage for water vapor transfer ($r_{a,f} = 2r_{a,f,h}$). See list of symbols for other parameters definition. Numbers (1), (2) and (3) denote the three soil reservoirs related to evaporation components *f* (main foliage), *vs* (vegetated soil) and *bs* (bare soil).

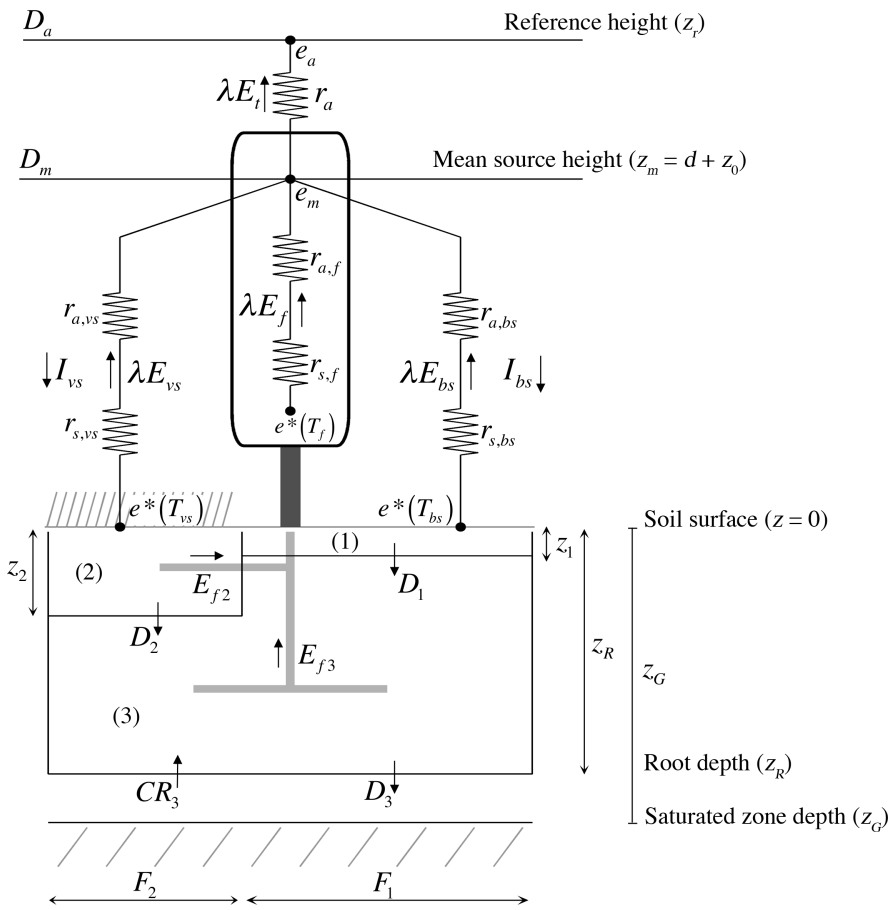

Fig. 2. Time series of meteorological variables, as measured during the simulation period, and used for model forcing. Gray shaded bars show periods of evaporation measurements used for model validation. (a)-(b) Daily incident solar radiation; (c)-(d) daily mean air temperature; (e)-(f) daily mean relative humidity; (g)-(h) daily mean wind speed; (i)-(j) daily accumulated precipitation. Also, simulated LAI_f (Eq. (37)) and estimated $CLAI_{vs}$ are shown in (k)-(l). Circles in (l) are LAI_f measurements. Shaded intervals in (c) to (h) represent daily minimum and maximum values. Abscise labels denote the beginning of each month.

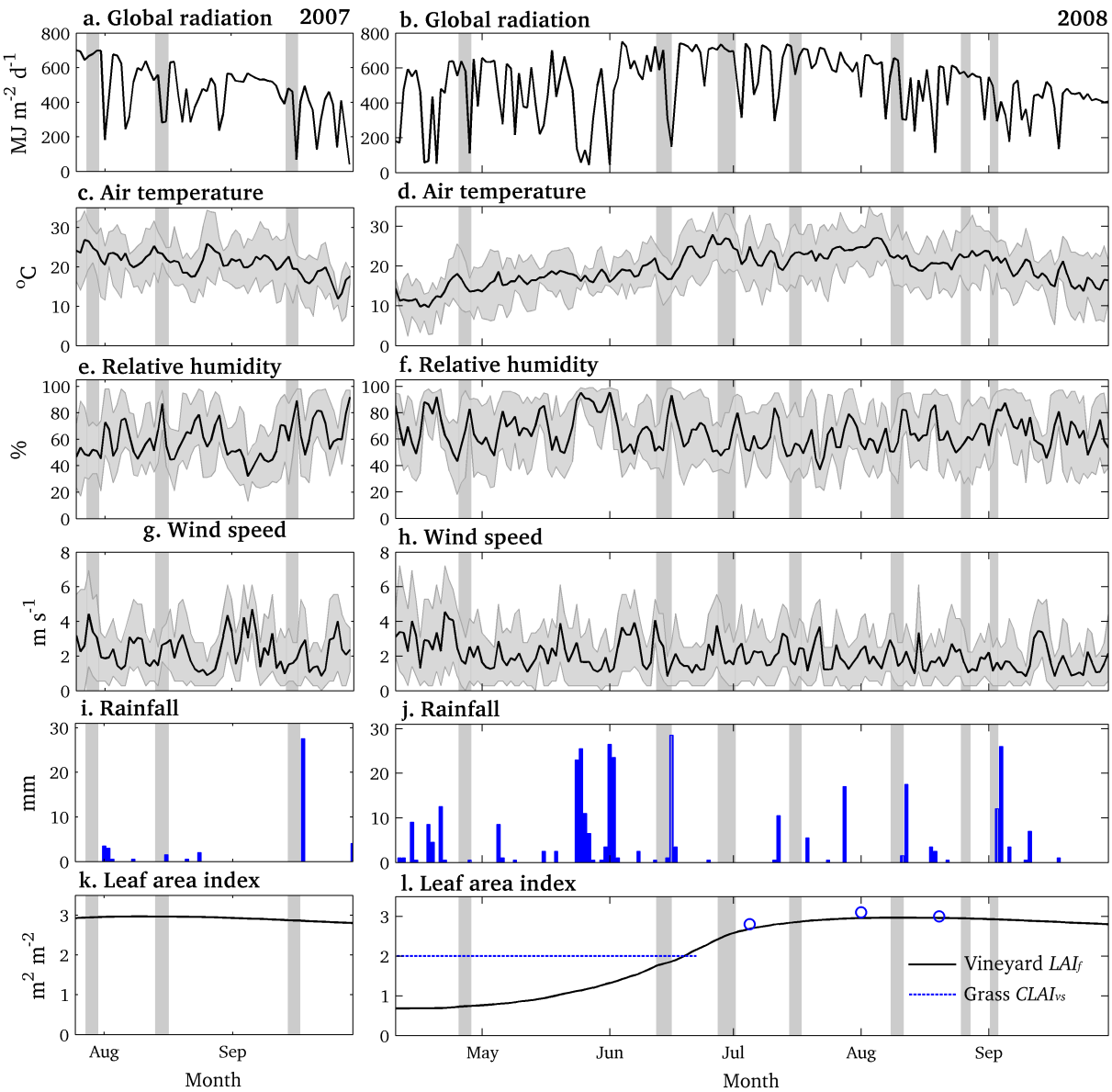

Fig. 3. Scatter plot of hourly measured and simulated total latent heat flux (λE_t).

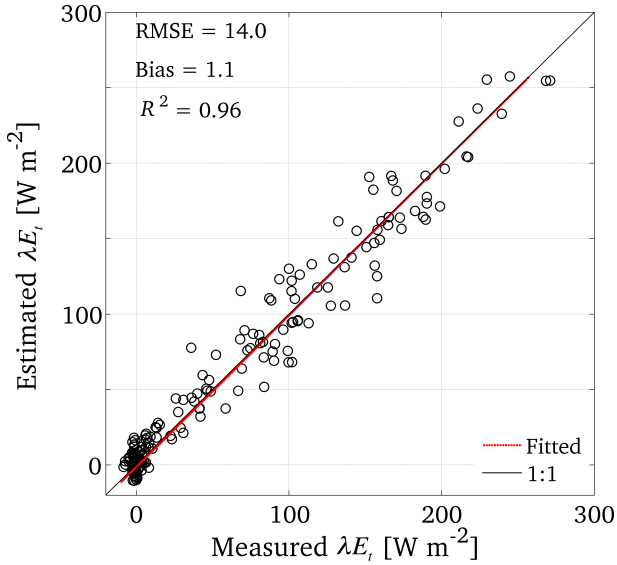

Fig. 4. Time series of simulated (lines) and measured (circles) hourly latent heat flux (λE_t) for eight observation days.

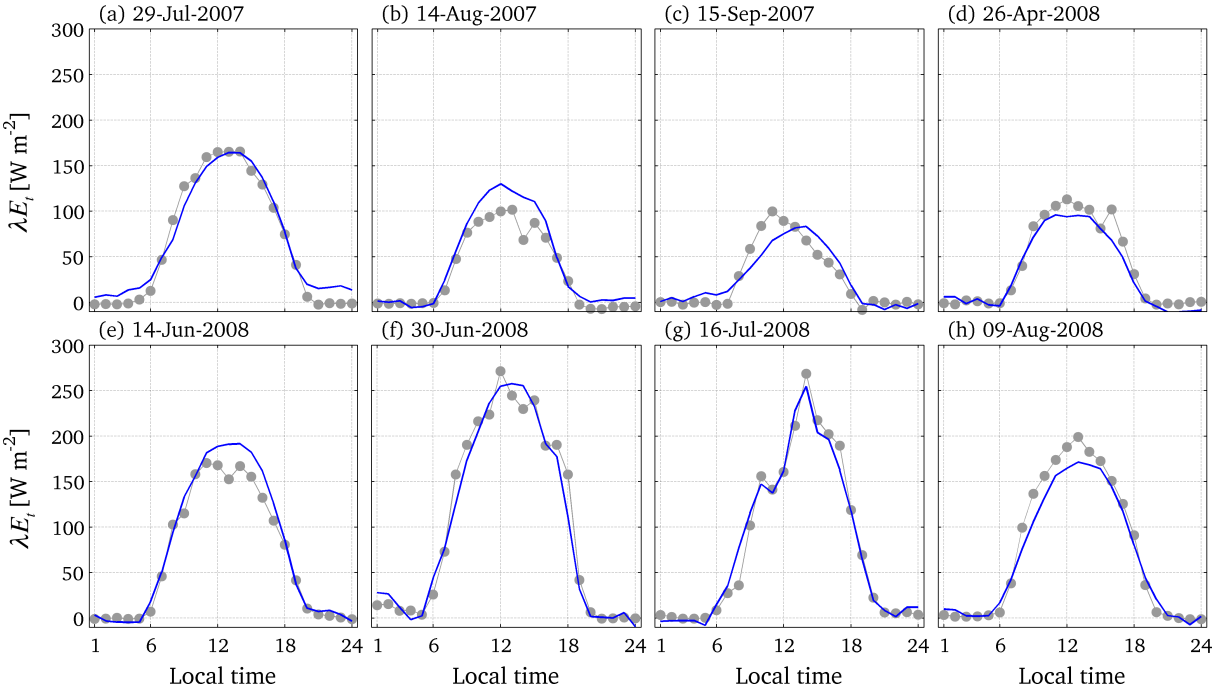

Fig. 5. Scatter plot of daily (a) total evaporation (E_t) and (b) soil water content (θ) as measured and as simulated by the model. In (a) only days with 24 hours of measurements were included.

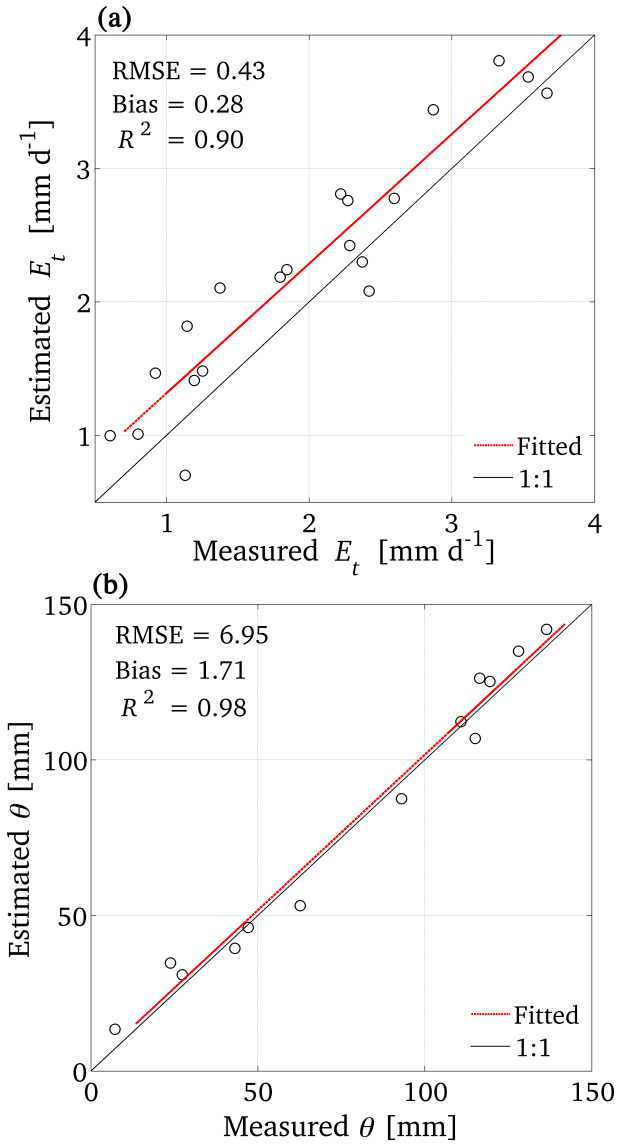

Fig. 6. Time series of (a) simulated (line) and observed (circles) daily total evaporation, and (b) simulated (line) and observed (circles) integrated profile volumetric soil water content. Abscissa labels denote the beginning of each month.

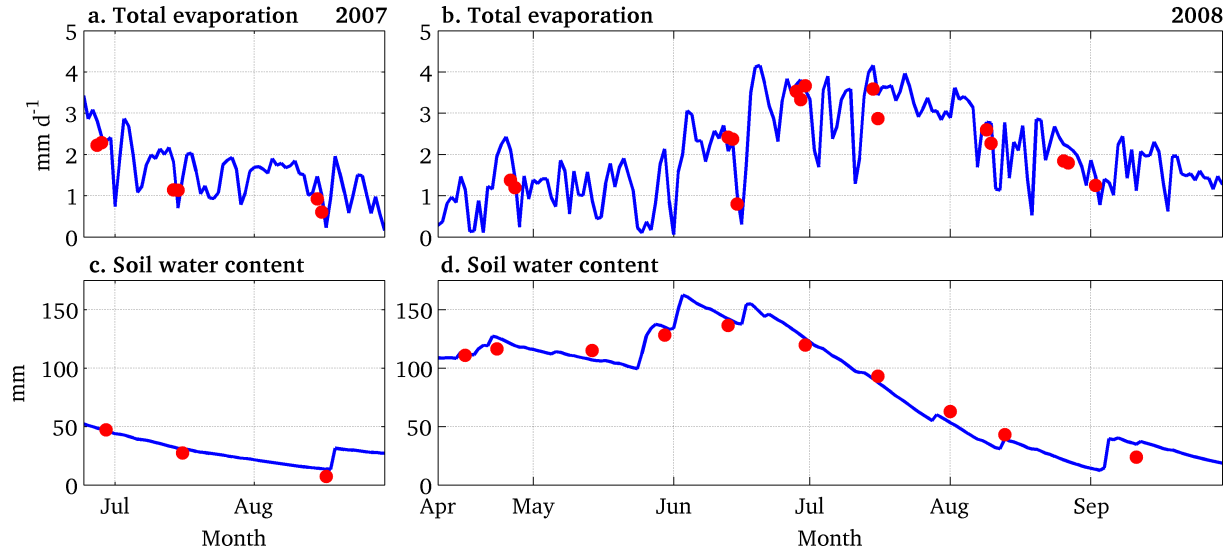

Fig. 7. Capillary flow (contours in mm d^{-1}) between saturated zone and reservoir (3) as a function of the distance between water table (z_G) and root zone depth (z_R) and soil water content of reservoir (3). Upward flow is taken as positive values.

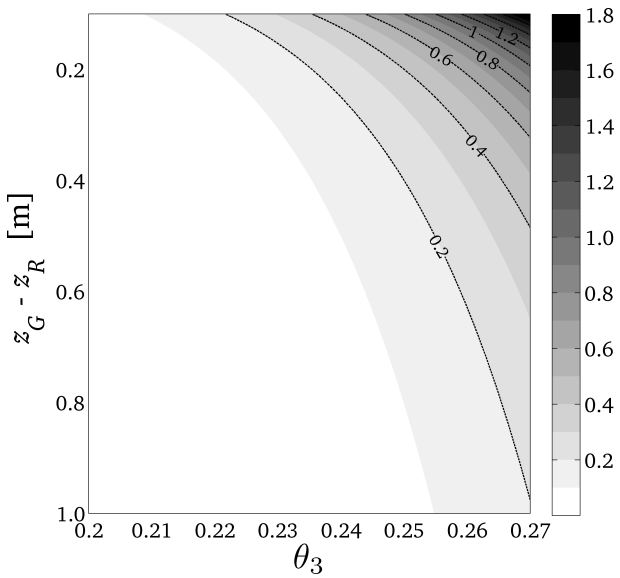
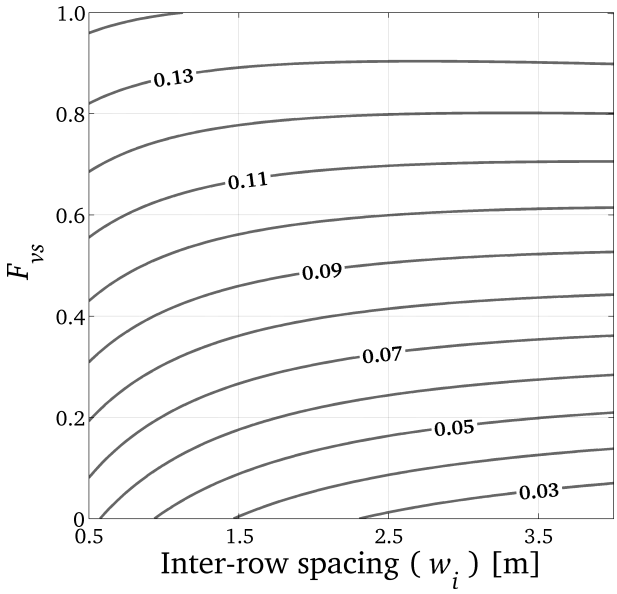
Fig. 8. Simulated total evaporation (contours in mm h^{-1}) as a function of the spacing between vine rows w_i and the grass cover fraction F_{vs}.